STUDY OF GENOME PACKAGING USING SINGLE – MOLECULE MANIPULATION AND IMAGE METHOD

LIU YINGJIE

A THESIS SUBMITTED

FOR THE DEGREE OF Ph.D OF PHYSICS

DEPARTMENT OF PHYSICS
NATIONAL UNIVERSITY OF SINGAPORE
October, 2009

Acknowledgement

The works described in this thesis was carried out in the Biophysics & Single-molecule manipulation Lab, National University of Singapore (NUS), from August 2005 to July 2009, and was supported by research scholarship from the Physics department of NUS.

I would like to thank Dr. Yan Jie, my supervisor, for all his guide, help, support and encouragement when I was in his group for the past 4 years. Without these, I would not have made so many achievements and it is an interesting and enriching experience for doing research and study in Biophysics & Single-molecule manipulation Lab.

I am grateful to Dr. Chen Hu, Dr. Fu Hongxia, Dr. Fu Wenbo, Law Dingying and all my group members for their help and suggestion during the period. I am also grateful to my collaborator, Prof. Peter Dröge, Prof. Leong-Hew Choy, Prof. Linda Kenney, and Dr. Wu Jinlu for their excellent works and discussions.

Table of Content

Acknowledgement ..... **i**

Table of Figures ..... **iv**

Summary ..... **viii**

Chapter 1. Introduction: Architectural Protein in Prokaryotes and Eukaryotes **1**
1.1. References 14

Chapter 2. The techniques: Atomic Force Microscopy (AFM), Electrophoretic Mobility Shift Assay (EMSA), Transverse Magnetic tweezers **16**
2.1. Atomic Force Microscopy 16
2.2. Mica surface modification 19
2.3. Magnetic Tweezers 22
2.4. Electrophoretic Mobility Shift Assay 25
2.5. References 26

Chapter 3. AFM study of scIHF-induced DNA bending **27**
3.1. Introduction of IHF 27
3.2. Methods 31
Procedure for APTES functionalization 31
Procedure for Glutaraldehyde functionalization. 31
AFM imaging of DNA-protein complexes. 31
3.3. Results 32
3.4. Discussion 39
3.5. References 41

Chapter 4. Single DNA study of VP15-DNA interaction **43**
4.1. Introduction 43
4.2. Methods 44
Electrophoretic mobility shift assay (EMSA) 44
Magnetic-tweezer Manipulation of VP15-DNA complex 45
4.3. Results 46
EMSA experiment confirmed that VP15 is a DNA-binding protein and it can package DNA cooperatively when the protein concentration exceeds a threshold value. 46
Magnetic tweezer (MT) experiments revealed that VP15 could compact DNA against certain forces when the protein concentration was larger than a threshold value. 49
AFM experiments revealed that VP15 packages DNA by making synergies

between remote DNA sites....52
4.4. Discussion....53
4.5. References....57

Chapter 5. Single DNA study of H-NS-DNA interaction....59
5.1. Introduction....59
5.2. Methods....61
Magnetic-tweezer Manipulation of H-NS-DNA complex....62
Atomic Force Microscope imaging....62
5.3. Results....63
Ionic strength and magnesium ion alter the mode of H-NS binding to DNA. 63
Magnesium acts as a switch between stiffening and bridging. 65
Stiffening results from cooperative H-NS polymerization along DNA. 68
During folding (bridging), large DNA hairpin structures form. 71
5.4. Discussion....73
5.5. Supplementary Data....76
5.6. References....77

Chapter 6. Conclusion....80

List of publications....85

Table of Figures

Fig. 1.1 [1] Cellular localization of the genome in cells from different kingdoms of lives.....3

Fig. 1.2 (Picture is copied from Karolin Luger's paper [8]) nucleosome core particle: ribbon traces for the 146-bp DNA phosphodiester backbones (brown and turquoise) and eight histone protein main chains (blue: H3; green: H4; yellow: H2A; red: H2B). The views are down the DNA superhelix axis for the left particle and perpendicular to it for the right particle. For both particles, the pseudo-twofold axis is aligned vertically with the DNA centre at the top. 6

Fig. 1.3 (Picture is copied from Karolin Luger's paper [8]). The central base pair through which the dyad passes is above the SHL0 label, (SHL, superhelix axis location). Each SHL label represents one further DNA double helix turn from SHL0. The complete histone proteins primarily associated with the 73-bp superhelix half are shown (interparticle tail regions are not shown). The two copies of each histone pair are distinguished as unprimed and primed copies, where the histone of the unprimed copy is primarily associated with the 73-bp DNA half and the primed copy with the 72-bp half. The 4-helix bundles are labeled as H3' H3 and H2B H4; histone-fold extensions of H3 and H2B are labeled as αN and αC, respectively; the interface between the H2A docking domain and the H4 C terminus as b; and

N- and C- terminal tail regions as N or C. 7

Fig. 1.4 (Pictures are copied from Kerren K. Swinger et al's paper [11]) HU+DNA and IHF+DNA cocrystal structures. 9

Fig. 2.1 Schematic diagram of an Atomic force microscope. 18

Fig. 2.2 Pictures of AFM in our lab. 19

Fig. 2.3 Schematic histogram showing the modified mica surfaces. 21

Fig. 2.4 Schematic histogram of magnetic tweezers system. 23

Fig. 2.5 Picture of magnetic tweezers system, including microscope and micro-manipulator. 23

Fig. 2.6 Picture of flow channel and controlled magnet. The glass with a 200μL tube on its left side is the channel inside which the DNA is attached (in the right part of the picture). The force is controlled by changing the distance between the magnet (the black bricks) and the channel. 24

Fig. 3.1 Structure of IHF protein (Picture is copied from Phoebe A. Rice et al [2]). 28

Fig. 3.2 Structure of single-chain IHF (scIHF) [10] 30

Fig. 3.3 AFM images of attL DNA on mica surface 35

Fig. 3.4 Zoom-in images of wild-type IHF induced DNA bending. (The bright dot in the 2/3 part of DNA indicates a wild-type IHF in the expected location) 35

Fig. 3.5 Zoom-in images of scIHF2 induced DNA bending. (The bright dot in the 2/3 part of DNA indicates a scIHF in the expected location). 36

Fig. 3.6 Zoom-in images of scIHF2-K45αE induced DNA bending. (The bright dot in the 2/3 part of DNA indicates a scIHF2-K45αE in the expected location). 36

Fig. 3.7 Histogram of bending angle distribution. 37

Fig. 3.8 Histogram of bending angle distribution of Mg^{2+} dependence 37

Fig. 3.9 Zoom – in image of scIHF2-K45αE induced DNA bending in 20 nM Mg^{2+} solution condition (the bright dot in the 2/3 part of DNA indicates a scIHF2-K45αE in the expected location).....38

Fig. 3.10 Zoom – in image of scIHF2-K45αE induced DNA bending in 200 nM Mg^{2+} solution condition (the bright dot in the 2/3 part of DNA indicates a scIHF2-K45αE in the expected location).....38

Fig. 4.1 Electrophoretic mobility shift assay (EMSA). 48

Fig. 4.2 DNA folding dynamics under different forces and different VP15 concentrations. 51

Fig. 4.3 DNA unfolding dynamics under different forces and different VP15 concentrations. 52

Fig. 4.4 AFM images of linear phix174 DNA with and without VP15. (The height scale bar ranges from 0 – 2nm for Fig. 4.4 a - d and f, and from 3 – 8nm for e).....53

Fig. 5.1 Magnesium dependent binding modes of H-NS.....66

Fig. 5.2 H-NS interconverts between bridging and stiffening modes without being released from DNA. 70

Fig. 5.3 Imaging of DNA–H-NS complexes in the absence of or with low $MgCl^2$ concentration using Atomic Force Microscopy. 71

Fig. 5.4 Imaging of DNA–H-NS complexes in the bridging binding mode. 72

Fig. 5.5 Calcium substitutes for magnesium in stimulating the bridging/polymerization switch. 76

Fig. 5.6 Increasing the H-NS concentration dramatically reduces the DNA folding kinetics..... 76

Summary

The interaction between DNA and protein is of intense interest in biophysical research, especially the binding energy, DNA folding force, DNA elasticity and DNA-protein complex topography. These are important in genomic compaction and function for all organisms.

My Ph.D research focuses mainly on the understanding of how these proteins perform their functions and on the study of DNA-protein interactional process by using magnetic tweezes and Atomic Force microscopy (AFM). Magnetic tweezers is widely used in single DNA manipulation experiment and to study the dynamical process of DNA-protein interaction. The static information, such as topography, of DNA-protein complexes can give the most direct evidence to assumptions which are derived from single DNA manipulation experiments. The AFM is used to give structural details of DNA-protein complexes at the nano scale.

In this thesis, I will describe 3 kinds of proteins that have been studied in my lab: Integration Host Factor (IHF), VP15 from White Spot Syndrome Virus (WSSV) and Histone-like Nucleoid Structural Protein (H-NS). All of them are DNA binding protein and have large influence on the DNA topography. Our main interest is placed on the topography of DNA-protein complexes, critical folding force and protein function under different ionic condition.

VP15 shows the strongest DNA compacting ability among the 3 kinds of proteins with a critical folding force up to 5 pN. However, IHF and H-NS are more interesting

than VP15 in that their functions are ionic concentration dependent. The bending ability of scIHF, presented by bending angle distribution of DNA-IHF structure, depends on Mg^{2+} concentration. The most notable protein, H-NS, shows two switchable functioning modes according to whether Mg^{2+} or Ca^{2+} concentration is above certain value and two distinctly different DNA-H-NS structures are found using AFM.

Chapter 1. Introduction: Architectural Protein in Prokaryotes and Eukaryotes

DNA (deoxyribonucleic acid) is a nucleic acid that contains genetic information used to influence the development and evolution of all living organisms. Because each base pair on DNA is negatively charged and there is static repulsive force among these base pairs, DNA can be regarded as a semi-flexible polymer whose effective volume depends mostly on its persistence length when there is no compacting factor present. The persistence length is a mechanical property of the semi-flexible polymer and it is defined, formally, as the length over which correlation between the orientations of two connected hypothetical segments is lost. Therefore, a stiff polymer is expected to require more space than a flexible one. One of the major challenges faced by many cells is how to effectively reduce the volume of its genome by several orders of magnitude while still retaining exactly all its genetic functionality and effectiveness. For example, most of the *Escherichia coli* cells are about 2 μm long and 0.5μm wide, but their chromosomal DNA molecules have a contour length of approximately 2 mm. In absence of restriction, such a long DNA molecule would develop into a random coil whose volume is approximately 200 μm^3. However, the volume of an *E.coli* nucleoid is only around 0.5 μm^3, around 1/400 of the unconstrained DNA size (Fig. 1.1, copy from Martijn S. Luijsterburg et al [1]). Therefore, there must be some mechanisms to operate to compact the chromosomal

DNA sufficiently into the cell.

Macromolecular crowding is one of the mechanisms that are employed for compaction of DNA. In cells, large amount of RNAs and proteins are produced from transcription of genomic DNA and translation of mRNAs, respectively. The crowding condition caused by the high concentration of these macromolecules generates strong depletion/attraction forces [2, 3]. Depletion force is one kind of entropic forces which arises when there are differently-sized particles in the solution. The interactions among the excluded volumes of larger particles tend to yield large space between adjacent particles. In turn, these increases of volume accessible to smaller particles result in strong attractive forces that can cause significant conformation changes of all particles [4]. The concentration of RNAs and proteins in nucleoids and nuclei are within the range where depletion/attraction forces can occur and thus help to largely compact DNA. It is highly possible that these crowded macromolecules in the cell induce considerable self-association of DNA and contributes to genomic organization. Although depletion/attraction forces may contribute to the association of architectural proteins which has important effects on genomic folding, the resulting genome crowding results in only non-specific compaction. Thus, the role it plays in gene regulating function may not be as important as it does in genomic compaction.

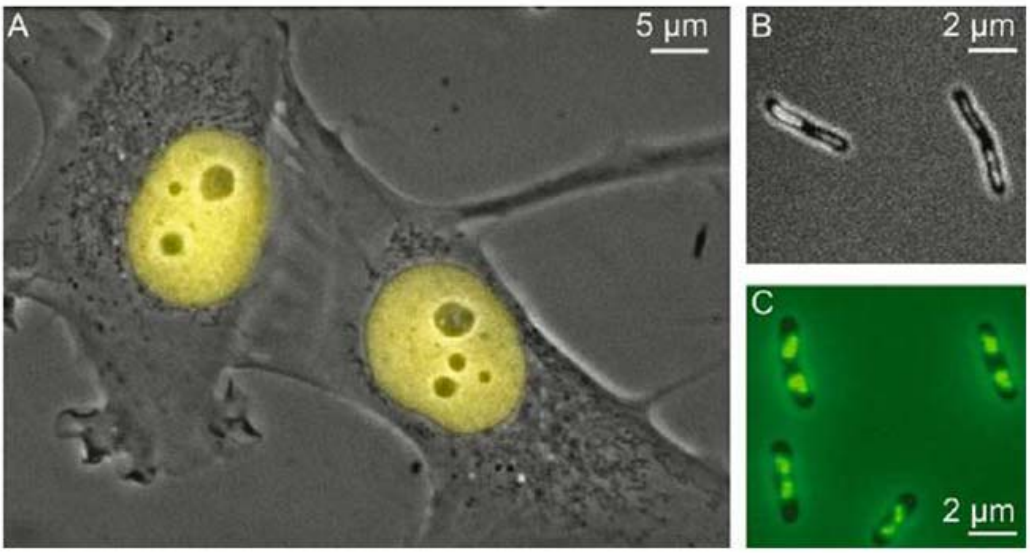

Fig. 1.1 [1] Cellular localization of the genome in cells from different kingdoms of lives.

A) Microscopic image of a living human fibroblast (phase contrast) showing the nucleus by expression of a nuclear YFP-tagged DNA repair protein (DDB2).

B) Microscopic image of a living archaeal cell in late exponential phase of growth, showing the nucleoid by staining with DAPI and Microscopic image of a living bacteria cell (*E.coli*) in exponential phase of growth, showing the nucleoid by expression of GFP-tagged H-NS protein.

To perform biological function such as transcription, translation, repression and derepression, architectural chromosomal proteins are necessary and most of them are small (~10 kDa), basic and have specific functions after binding to DNA. According to their effects on DNA, these proteins can be roughly divided into 3 classes: DNA wrapper, DNA bender and DNA bridger. This classification is based mostly on the topographies of DNA-protein complexes, and it sheds light on understanding the fundamental role that those DNA architectural proteins played in the organization and

regulation of the genome. Moreover, these architectural proteins show, to certain degree, conservative functionalities. Therefore, the proteins from one kind of organism can perform similar function as proteins from another organism. DNA compaction results generally from two modes: one is wrapping by histone/HMF protein in eukaryotes and some archaea [5], and the other is bending by HU/Sul7/Cren7/MC1 in bacteria and prokaryotes [6].

All kinds of Organisms have evolved their specific mechanisms to organize their genome and to compact it into different structures, like nucleoid in the prokaryotic cell and chromosomes in the eukaryotic cell.

However, the binding affinity of the architectural proteins to DNA can be influenced by many factors such as ionic concentration, pH value of the surrounding environment, temperature and also the native structure of DNA. For example, supercoiling DNA has high protein binding affinity, either by affecting the local DNA effective concentration through plectonemic formation which favors DNA bridging or by reducing the free energy that is required to bend or wrap the DNA [1].

Because of the static repulsive force between DNA base pairs, there is a limited number of ways in which DNA structure can be regulated. By inducing either bending or bundling formation on DNA, architectural proteins, while reducing the effective volume, introduce functional regulation on genome. A good example is the mentioned “Histone-like nucleoid structural protein” (H-NS) whose binding can occur in the specific promoter region, thus preventing the access of RNA polymerase or other proteins to perform their tasks such as transcription and DNA cutting [7].

In eukaryotes, the compaction and regulation is mainly carried out by one kind of major proteins called histone proteins, which have histone-fold of 3-hydrophobic α-helices. The histone proteins interact with DNA by inserting their arginine residues into the minor groove every helical turn on DNA [8]. Generally, there exit 4 kinds of core histones: H2A, H2B, H3 and H4. They function by composing a "histone octamer" rather than work alone. First, two H3-H4 connect together through their histone-fold, and then, two H2A-H2B associate with this "core" to form the octamer ~146 bp (basepair) of 200bp DNA wrap around the histone complex forming the nucleosome, which is widely known as a repressor to DNA-transacting processes such as transcription (Fig. 1.2 and Fig. 1.3). It has been reported that the DNA is able to transiently detach from the octamer surface for 40-50ms, allowing proteins to access the previously warped DNA. This may be one of the forms in which the transcription starts.

The major DNA compaction mode in eukaryotes is histone induced DNA wrapping. However, when it comes to bacteria and prokaryotes, the dominant mode of organizing DNA is bending and bridging because these organisms lack histone protein. In virus and prokaryotes, there is another type of proteins which is referred to as nucleoid-associated proteins (NAPs), because they also help DNA compaction by binding to DNA but lack structural resemblance with histones.

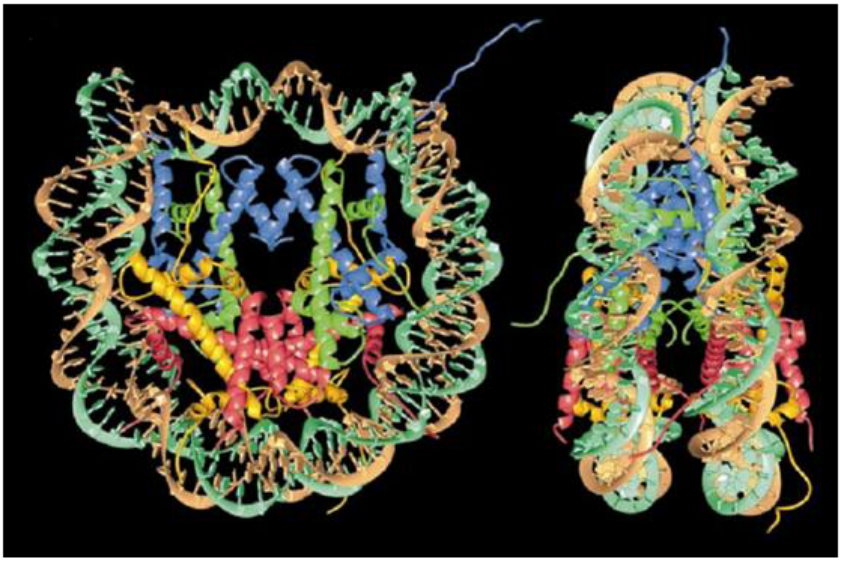

Fig. 1.2 (Picture is copied from Karolin Luger's paper [8]) nucleosome core particle: ribbon traces for the 146-bp DNA phosphodiester backbones (brown and turquoise) and eight histone protein main chains (blue: H3; green: H4; yellow: H2A; red: H2B). The views are down the DNA superhelix axis for the left particle and perpendicular to it for the right particle. For both particles, the pseudo-twofold axis is aligned vertically with the DNA centre at the top.

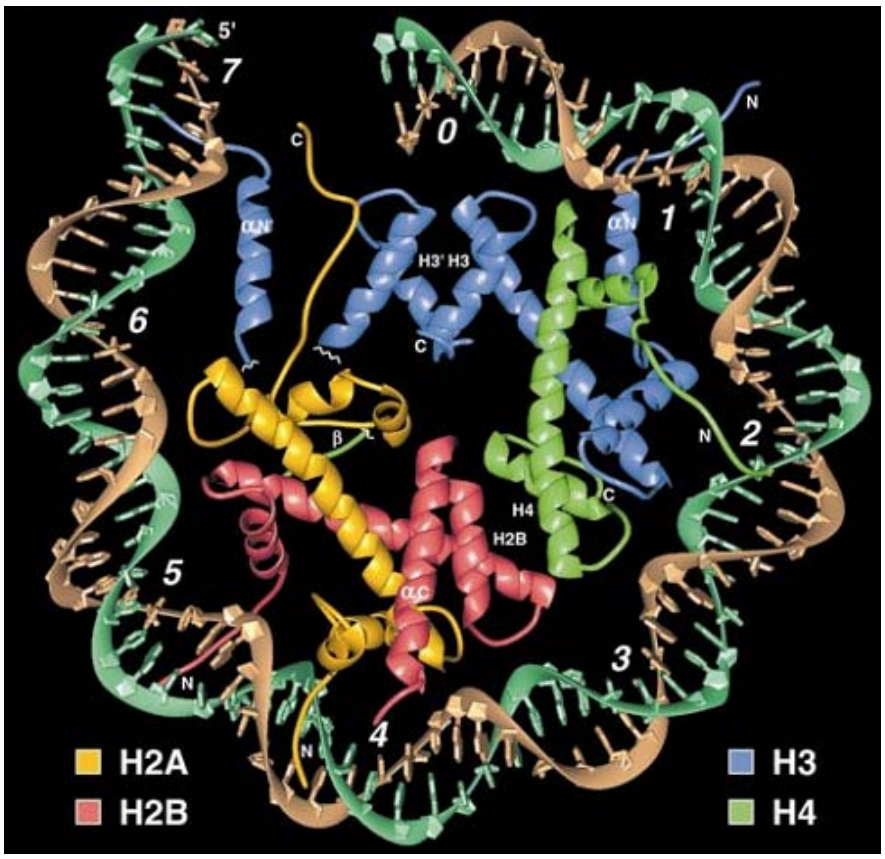

Fig. 1.3 (Picture is copied from Karolin Luger's paper [8]). The central base pair through which the dyad passes is above the SHL0 label, (SHL, superhelix axis location). Each SHL label represents one further DNA double helix turn from SHL0. The complete histone proteins primarily associated with the 73-bp superhelix half are shown (interparticle tail regions are not shown). The two copies of each histone pair are distinguished as unprimed and primed copies, where the histone of the unprimed copy is primarily associated with the 73-bp DNA half and the primed copy with the 72-bp half. The 4-helix bundles are labeled as H3' H3 and H2B H4; histone-fold extensions of H3 and H2B are labeled as αN and αC, respectively; the interface between the H2A docking domain and the H4 C terminus as b; and N- and C-terminal tail regions as N or C.

Besides genomic organization and compaction, these proteins are involved in a broad range of DNA transacting processes such as replication, recombination,

transcription and DNA repair. The proteins from bacteria and prokaryotes can generally be divided into two types according to their functions on DNA: DNA bender and DNA bridger. The HU/IHF family is the best studied DNA bender [9, 10]. This kind of protein is dimeric and composed by a compact core of α-helices and two flexible β-ribbon arms. The two arms emanate from α-helices and insert into the minor groove of DNA to introduce a bending around the protein with an angle up to 160°。HU shows a preferential binding to structural distortion on DNA sequence [11] (Fig. 1.4), such as gaps, nicks Besides, HU can recognize pre-existing bending and help to stabilize it [12, 13]. Moreover, the number of HU that binds to DNA can influence the bending angle and the extent to which DNA is compacted [14].

IHF has similar function on DNA as HU but it also shows DNA sequence specificity and non-specific binding [15] [16]. However, the bend induced by HU is not as rigid as the one induced by IHF and it appears that HU can introduce a range of different bending angles similar to high mobility group (HMG) protein in eukaryotes.

Another widely studied DNA bender is Fis, which is shown to contribute significantly to nucleoid compaction both by first binding non-specifically to DNA and then bending or looping DNA [17]. DNA loop formation is another function introduced by DNA bender and DNA bridger. The DNA loops are one kind of nucleoid territories. Their structures are dynamic and the boundaries are distributed in a random manner [18]. The different boundaries distribution along DNA can preserve the superhelicity of the genome but allow some of them to relax when proteins access DNA to perform their genomic function.

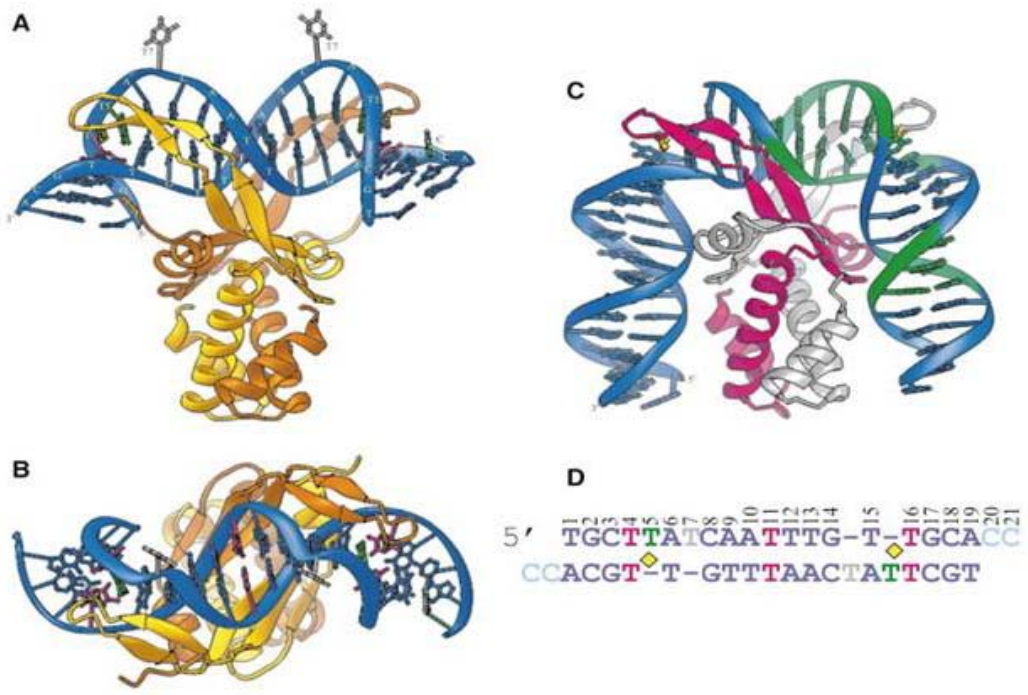

Fig. 1.4 (Pictures are copied from Kerren K. Swinger et al's paper [11]) HU+DNA and IHF+DNA co-crystal structures.

A) Ribbon diagram of the HU+DNA complex. The protein homodimer is in gold and orange, with intercalating proteins in yellow. Nucleotides are colored as described in (D).

B) The HU+DNA complex viewed from the top.

C) Structure of IHF bound to the H' site from phage I (Rice et al, 1996). The a subunit is white and the b subunit is pink and the intercalating prolines are yellow. The DNA is blue except for the consensus sequence which is green.

D) The sequence of the DNA substrate in TR3 with the three: T:T mismatches in pink and four unpaired "T"s in gray and green. The "T"s are fipped out of the duplex and make crystal packing contacts in the structure, while the green "T"s remain stacked. The yellow diamonds indicate sites of proline intercalation. The light blue "C"s are partially disordered in TR3 structures.

Another function of DNA bridging proteins is to cause dynamic cross linker between DNA strands which is either from one or several DNAs, forming a bundling

structure or large DNA – protein complexes. The representative of DNA bridgers is H-NS (Histone-liked nucleoid structural protein) which is found in *E.coli* and have been wildly studied. H-NS is a small abundant prokaryotic protein that organizes chromosomal DNA and plays an important role in gene silencing. It serves as a negative regulator and represses the expression of many genes which are involved in bacterial adoption to environmental change [19]. H-NS is present at 20,000 copies per cell and binds preferentially to A-T rich segments on DNA. It is composed of 3 parts and each has different function. The C-terminal domain (residues 90-136) binds DNA, while the N-terminus (residues 1-64) is involved in H-NS dimerization. The two domains are connected via an unstructured linker which is comprised of residues 65-89. H-NS exists as a dimer and has the ability to self-associate, forming higher order oligomers. With the two DNA binding sites, H-NS dimmer can interact with two DNA strands simultaneously [9]. Recent research has shown that H-NS has no DNA sequence preference but does have high affinity to AT rich parts [20]. By binding to the promoter region of many genes, H-NS can inhibit RNA polymerase and other proteins from accessing, thus interfering with transcription initiation. In this situation, H-NS functions as a repressor, silencing selectively specific genes or regions of chromosome, and as coordinator acting in concert with other transcription factors. Recent detailed research suggests that H-NS binds first to nucleating high-affinity sites separately, and then, dimmer – dimmer interaction leads to H-NS polymerization that results eventually in the formation of a supercoiled intertwined filament containing two DNA duplexes connected by protein bridges, constraining a DNA loop

[20]. The bundling DNA filament covered with H-NS nucleation would silence an extensive region of genes and operons. Seperate biophysical studies have revealed how H-NS dimers can bridge DNA and how the cooperative polymerization can happen and block transcription initiation[21].

When the network of DNA – H-NS complexes forms, DNA is sequestered from promoters which are regulated. When the surrounding environment changes, such as a decrease in ionic concentration, lack in food supply or temperature variation, in adaption to the new condition, H-NS proteins should leave from or attach to specific promoter sites. This leads to the hypothesis that there may be a structural reorganization of the nucleoid. The factor is receptive to signals from changed environmental conditions. Another possibility is that H-NS can act as an environmental sensor by changing its cooperative mode leading to new DNA - protein complexes (This effect has been showed by our group). According to our results, when Mg^{2+} is present, H-NS behaves as a DNA compactor, comparing to function as a DNA stiffener in absence of Mg^{2+}, and this will be discussed in detail in a later chapter.

To date, the mechanism and function of how nucleoid-associated proteins (NAPs) compact and regulate genomic expression is still unclear. Besides, none of these protein functions alone in DNA compactions, which is totally different from the situation in eukaryotes where the histone protein contribute exclusively to DNA compaction. Although, in *in vitro* experiments all NAPs clearly exhibit the ability to condense DNA, while in *in vivo* experiments, the effect from individual protein alone

is limited. For example, bacteria lacking one of the NAPs usually have subtle phenotypes, which suggests there is an overlap among the protein functions and the role of one protein can be compensated by another.

Another important phenomenon is that the expression level of nucleoid-associated proteins depends largely on cell growth phase. T. A. Azam et al analyzed 12 nucleoid – associated proteins at different cell growth phases [22]. The result showed that during exponential growth, some proteins are absent and become abundant during the stationary growth, or vice versa. This may be a possible explanation of how the cell can meet the requirement fro high levels of transcription and translation during growth and how to protect its genome when the stationary phase comes. The different expression level at different cell growth phage gives hint to model DNA structure according to the growth condition. For example, cell increases the Fis concentration to stimulate the transcription of stable RNA operons during growth and expresses Drp to bind extensively on genome to stop transcription at stationary phase. In order to switch between compacting and relaxed states, some of the nucleiod – associated proteins have definite genome condensing capability while some of the proteins have dual function and can act either as compacting agent or as antagonists. For example, Fis and IHF, which are DNA benders, can de-repress the impeditive effect of H-NS at specific promoters. HU exhibits a similar ability using a different mechanism which is to compete for preferential binding sites. However, more complex mechanisms may exist and require many proteins to work cooperatively in *in vivo* condition since there are hundreds of proteins inside a cell.

As mentioned before, DNA loops are dynamical and have random boundaries. If the DNA bending protein does not require specific binding region, the loop formation is likely to reform in a different manner every time, and this sheds light on the dynamics of bacterial chromosomal organization.

DNA benders, DNA wrappers and DNA bridgers are widespread and most of them show little structural conservation but only functional similarity. Genome organization and compaction is vital to organisms but there is diversity in what type of architectural protein that the organisms have developed. However, the number of options to reduce the volume of genome seems limited and they are used in all forms of living organisms.

In later chapters, organization and compaction of DNA by 3 kinds of proteins are studied using Atomic Force Microscope (AFM) and transverse magnetic tweezers. The results indicate that the protein from virus has a simpler function compared with the proteins from prokaryotes. IHF introduces different DNA bending angles according to variation of Mg^{2+} concentration and H-NS, being more complicated, has two binding modes which lead to two distinct DNA structure.

1.1. References

[1] M. S. Luijsterburg, M. F. White, R. v. Driel, and R. T. Dame, Critical Reviews in Biochemistry and Molecular Biology **43**, 393 (2008).

[2] D. Marenduzzo, K. Finan, and P. R. Cook, Journal of cell biology **175**, 681 (2006).

[3] R. Hancock, Journal of structural biology **146**, 281 (2004).

[4] P. Nelson, W.H Freeman and Company, New York (2004).

[5] M. S. Luijsterburg, M. C. Nooma, G. J. L. Wuite, and R. T. D. a, Journal of structural biology **156**, 262 (2006).

[6] K. K. Swinger, and P. A. Rice, Current Opinion in Structural Biology **14**, 28 (2004).

[7] C. J. Dorman, Nature reviews. Microbiology **5**, 157 (2007).

[8] K. Luger, A. W. Mäder, R. K. Richmond, D. F. Sargent, and T. J. Richmond, Nature **389**, 251 (1997).

[9] M. S. Luijsterburg, M. C. Nooma, G. J. L. Wuite, and R. T. Dame, Journal of structural biology **156**, 262 (2006).

[10] K. K. Swinger, and P. A. Rice, Current Opinion in Structural Biology **14**, 28 (2004).

[11] K. K. Swinger, K. M. Lemberg, Y. Zhang, and P. A. Rice, EMBO journal **22**, 3749 (2003).

[12]H. Tanaka, N. Goshima, K. Kohno, Y. Kano, and F. Imamoto, Journal of Biochemistry **113**, 568 (1993).

[13]N. Goshima, Y. Kano, H. Tanaka, K. Kohno, T. Iwaki, and F. Imamoto, Gene **141**, 17 (1994).

[14]H. Shindo, A. Furubayashi, M. Shimizu, M. Miyake, and F. Imamoto, Nucleic Acids Research **20**, 1553 (1992).

[15]P. A. Rice, S.-w. Yang, K. Mizuuchi, and H. A. Nash, Cell **87**, 1295 (1996).

[16]B. M. J. Ali, R. Amit, I. Braslavsky, A. B. Oppenheim, O. Gileadi, and J. Stavans, Proceedings of the National Academy of Sciences **98** (2001).

[17]D. Skoko, J. Yan, R. C. Johnson, and J. F. Marko, Physical review letters **95**, 208101 (2005).

[18]L. Postow, C. D.Hardy, and J. Arsuaga, Genes & Development **18**, 1766 (2009).

[19]C. J. Dorman, Nature reviews. Microbiology **2**, 391 (2004).

[20]B. Lang, N. Blot, E. Bouffartigues, M. Buckle, M. Geertz, C. O. Gualerzi, R. Mavathur, G. Muskhelishvili, C. L. Pon, S. Rimsky, S. Stella, M. M. Babu, and A. Travers, Nucleic Acids Research **35**, 6330 (2007).

[21]E. Bouffartigues, M. Buckle, C. Badaut, A. Travers, and S. Rimsky, nature structural & molecular biology **14**, 441 (2007).

[22]T. A. Azam, A. Iwata, A. Nishimura, S. Ueda, and A. Ishihama, Journal of Bacteriology **181**, 6361 (1999).

Chapter 2. The techniques: Atomic Force Microscopy (AFM), Electrophoretic Mobility Shift Assay (EMSA), Transverse Magnetic tweezers

2.1. Atomic Force Microscopy

DNA, although very long, has a diameter of merely 2 nm which makes it impossible to be visualized by traditional microscopy. To see nano-sized DNA-protein complexes, SPMs (scanning probe microscopy) are widely applied in biological research. For instance, SEM (scanning electron microscope) and TEM (transmission electron microscope) are able to show clear images for minimum sample-size 10nm and many images of nucleus and nucleoid has been reported. However, there are some drawbacks for these EM imaging techniques. In order to acquire high resolution images, both the samples and substrates must be conductive. Moreover, the sample should be fixed, i.e. not moving freely on the surface. These require the chemical modification of substrates, which may induce unknown artificial results on the DNA-protein complexes such as DNA condensation and protein repulsion. Another problem is the surface extension force that stretches DNA when a sample is placed in the vacuum chamber.

These limitations were addressed with the invention of atomic force microscopy (AFM) which has some special advantages when compared to normal Electron

Microscopy (EM). First, it does not require the sample to be conductive and is capable of measurement of the topography of almost any kind of surfaces. Second, AFM uses a reflection laser from the probe that scans the sample by gently “touching” the surface. This can effectively reduce the perturbation and damage of biological samples when observed with EM.

The main components of a modern AFM are mainly a cantilever, a laser beam deflection system, a piezoelectric scanner nose, an electronic control unit and a computer that controls the whole system (Fig. 2.1).

There are two primary scanning modes of AFM: contact mode and tapping mode (or AC mode), according to whether the probe contacts with the sample surface constantly or not.

In contact mode, the cantilever probe is brought into physical contact with the scanned sample and tracks the topographic changes as the probe moves along the surface. This causes the deflection in the cantilever to deflect which then change the position of the reflecting laser on a four quadrant photodetector. The change is then calculated and converted to the morphological change by the electronic control unit and computer program.

When the probe moves across the samples surface under the contact mode, the sharp tip and the lateral component can cause damage to soft or fragile samples, especially in the case of biological specimens. In these cases, tapping mode is preferred. Under tapping mode, the probe is not continuously in contact with sample surface like that in contact mode. Instead, the probe oscillates during scanning, and a

force interaction between the probe and the sample causes a change in the resonant frequency and oscillation amplitude of the vibrating cantilever. Either of them is then used to control the tracking of the probe over the surface. This mode allows the same high sensitivity compared to contact mode without causing damage to the soft samples.

In our experiment, tapping mode AFM was used to scan DNA-protein complexes on differently modified mica surfaces (Fig. 2.2).

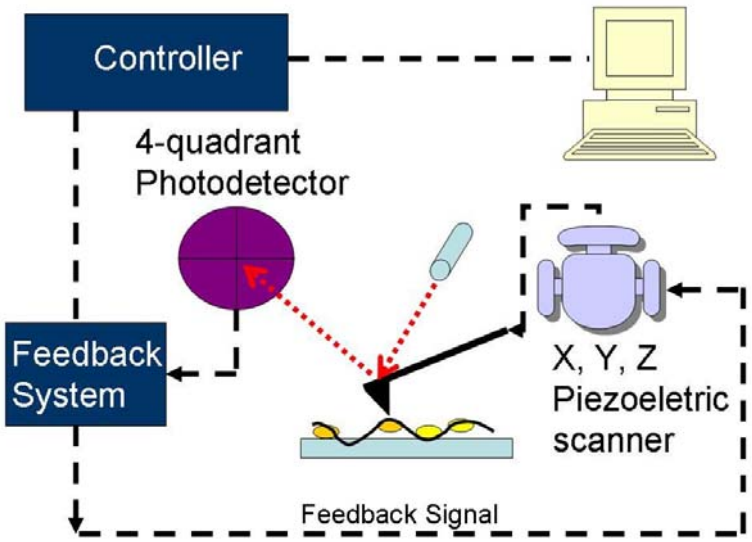

Fig. 2.1 Schematic diagram of an Atomic force microscope.

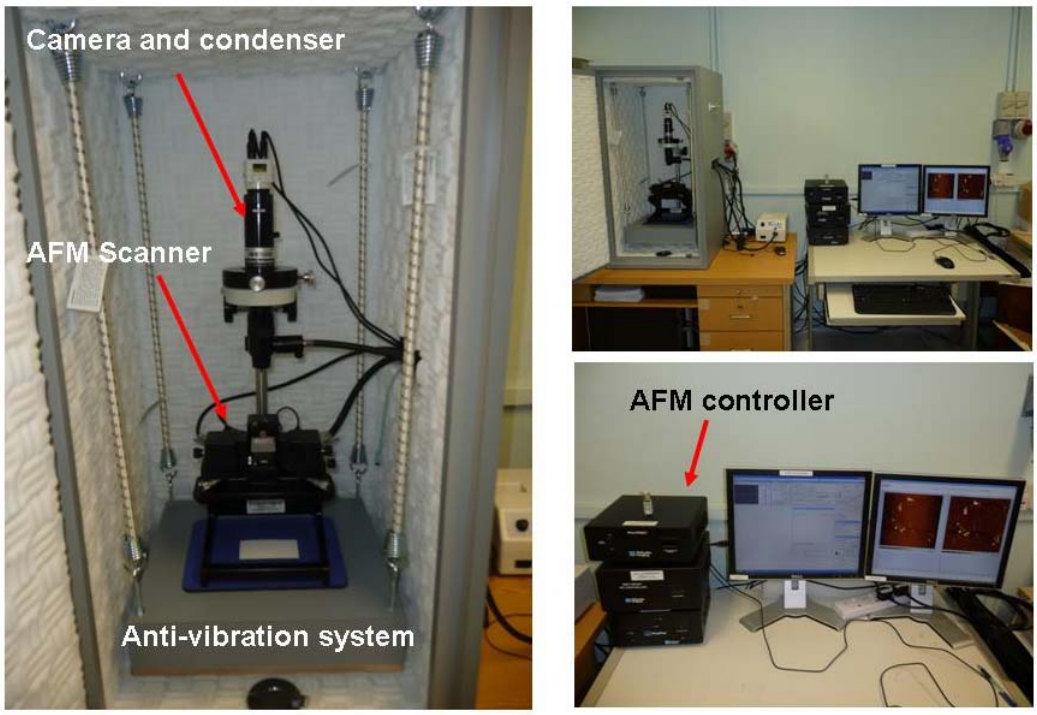

Fig. 2.2 Pictures of AFM in our lab.

All the AFM images are acquired using tapping mode scanning. The cantilevers are made of silicon with resonance frequency at 240 kHz to 300 kHz and spring constant at ~40N/m. For stability and quality reasons, all the scans are performed under 1 Hz line rate and 512 x 512 resolution.

2.2. Mica surface modification

AFM is proven to be an extremely useful instrument in biological research, especially in the study DNA-protein interaction. Despite its advantages and the progress made, a major handicap stems from the unreliable nature of the deposition

process in which only a small amount of sample can be found on the mica surface.

DNA has a diameter of merely 2 nm and the proteins have normal sizes of 1~3nm, therefore, any surface roughness larger than 2 nm will have great influence on the scanning results, hindering useful information of conformational details. Mica is a good candidate for DNA-protein complex imaging because of the smoothness of its surface (height fluctuation is less than 1 Å). However, the issue is that when contacting with water, the mica surface becomes negatively charged, thus DNA is repelled away from the surface because it is also negatively charges. Any washing and drying process leave little DNA for imaging.

To date, most of the surface modifications are based on the electrostatic attachment of bio-samples to an oxide surface. A common method is to use bivalent ion, such as Mg^{2+} or Ca^{2+}, to place positive charges on the mica surface serving as a bridge between the mica surface and DNA molecules (Fig. 2.3 A). However, these cations, while helping to bind DNA to the negatively charged surface, can also condense DNA by neutralizing the intrinsic charges of DNA, resulting in unpredictably compacting effect. Besides, bivalent ion effect on protein function is of great interest to scientists, so depletion of Mg^{2+} or Ca^{2+} is necessary and this prevents the application of saline fixation of DNA.

Another modification places amine on the mica surface by reaction with aminopropyltriethoxysilane (APTES) and the amine group can hold DNA tightly without bivalent ions (Fig. 2.3 B). Despite its excellent capability in adhering the DNA random coiled structure for AFM imaging, the APTES-modified mica has been

reported to lead to influence the morphology of DNA-protein structure [1]. The reason is that most of the DNA associated proteins bind to DNA by electrostatic force so the positively charged mica surface can repel the proteins away from DNA by competition.

In order to maintain the samples that accurately reflect the morphology, glutaraldehyde is used to further modify the APTES-treated mica as reported in paper of Wang et al [1]. Glutaraldehyde forms stable adducts with lysine residues, which can interact with proteins instead of with DNA (Fig. 2.3 C). Through linkages to proteins which then hold DNA, the glutaraldehyde mica maintains liable structure of deposited DNA-protein complexes.

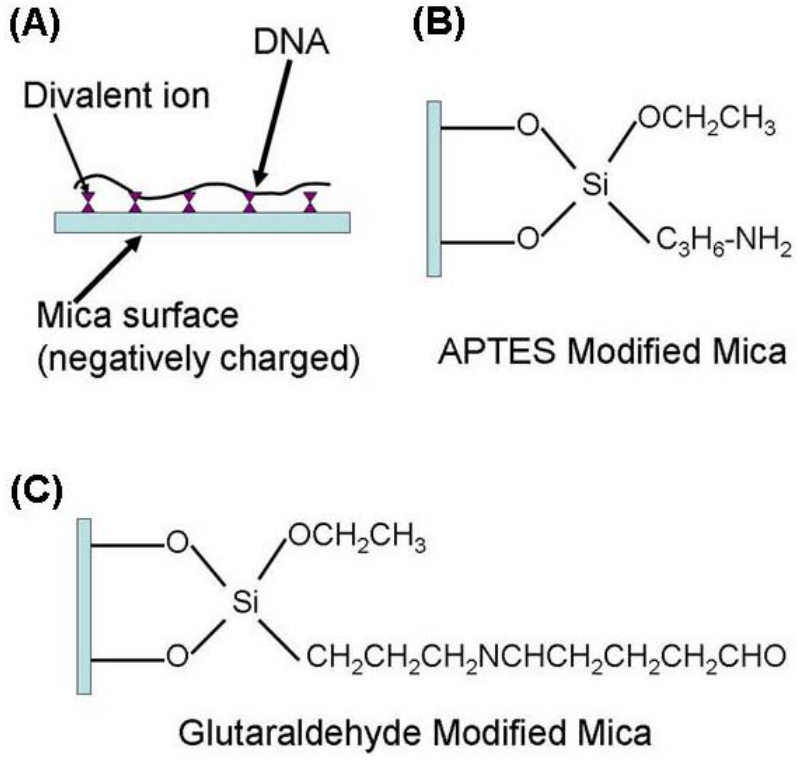

Fig. 2.3 Schematic histogram showing the modified mica surfaces.

2.3. Magnetic Tweezers

SPM (Scanning probe microscopy) can provide details of DNA-protein structures with high resolution, but lacks the liability to reveal details about the dynamical process and force response which are of great interest in biophysics. Magnetic tweezers is an instrument that, by using magnetic gradient field, exerts and measures the force on magnetic beads. Its typical application is in micromanipulation of single DNA molecules. In brief, the two ends of a DNA molecule (normally the 48.5kb -DNA) is first labeled with biotin- and digoxygenin-labeled oligonucleotides, respectively [2]. One end of labeled DNAs is then bound to a 2.8-micron-diameter paramagnetic bead and the other end to an edge of a thin $0^{\#}$ cover glass. By placing a magnet near the paramagnetic bead, a force stretching the tethering DNA molecules is applied on the bead, and the force is calculated from the measurement of the bead's Brownian motion transverse to the direction of the force using the equation: $F/L = k_B T/(\delta X^2)$. Here, L the extension of DNA; (δX^2) represents an average over the square of the bead transverse displacement; T is the temperature and the k_B is Boltzmann's constant. In our experiment, the range of force is from 0.1pN to 20pN. The force was applied on the focal plane of the objective, and the extension of DNA was determined by measuring the distance between the bead and the edge of the cover glass in the force direction. More detailed description of the experiment setup and reference will

be introduced in Chapter 4.

Using magnetic tweezers, it is possible to directly "observe" the biological process such as DNA folding and DNA stiffening. Development of the techniques for manipulation of single DNAs is of large interest to biological physicists and molecular biologists.

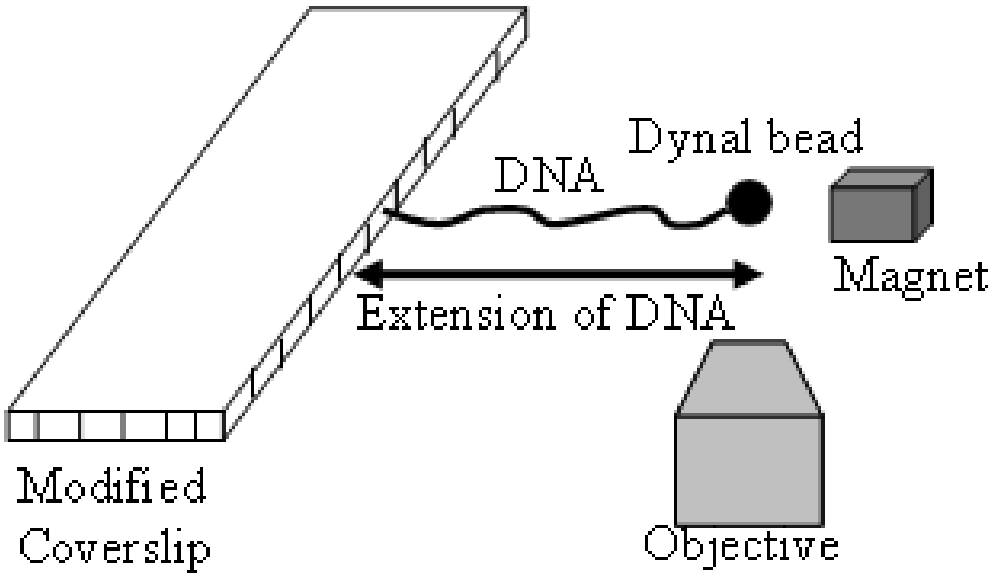

Fig. 2.4 Schematic histogram of magnetic tweezers system.

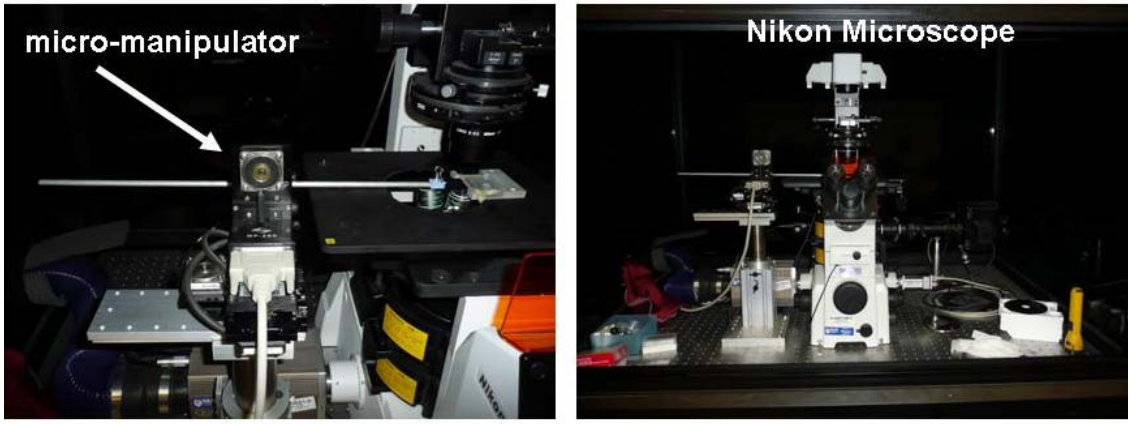

Fig. 2.5 Pictures of magnetic tweezers system, including microscope and micro-manipulator.

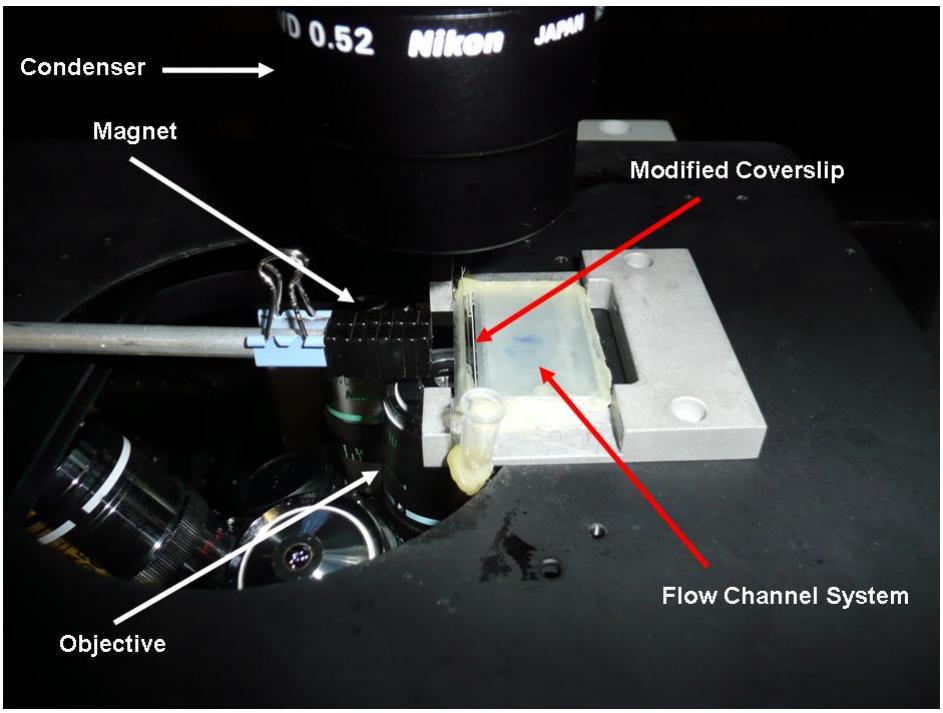

Fig. 2.6 Picture of flow channel and controlled magnet. The glass with a 200μL tube on its left side is the channel inside which the DNA is attached (in the right part of the picture). The force is controlled by changing the distance between the magnet (the black bricks) and the channel.

2.4. Electrophoretic Mobility Shift Assay

The Electrophoretic Mobility Shift Assay (EMSA), also referred to as gel retardation array or gel shift array, is a common technique used to characterize DNA-protein/RNA-protein interaction. It can determine whether a protein is capable of binding to a DNA/RNA and to cause structural changes of DNA/RNA such as bending, relaxing or cutting. EMSA is based on the observation that DNA-protein/RNA-protein complexes migrate through a nondenaturing agarose gel more slowly than free DNA/RNA fragments. In brief, the mixtures of DNA-protein/RNA-protein are loaded into agarose gel, and an external electric field is applied to drive complexes moving along according to the charge of the DNA-protein/RNA-protein mixture. The speed at which these molecules move in the gel is determined by their charges, sizes and their shapes. A control lane usually contains unbound DNA/RNA. Then, assuming that the protein binds to the DNA/RNA fragment, the lanes with DNA-protein/RNA-protein complexes will contain one or several different bands that represent the larger, less mobile complexes since the binding of protein can change not only charges, but also sizes and shapes of the complexes.

2.5. References

[1] H. Wang, R. Bash, J. G. Yodh, G. L. Hager, D. Lohr, and S. M. Lindsay, Biophysical Journal **83**, 3619 (2002).

[2] Smith, S. L. Finzi, and C. Bustamante, science **258**, 1122 (1992).

Chapter 3. AFM study of scIHF-induced DNA bending

3.1. Introduction of IHF

The assembly of specialized nucleoprotein structure (snups) plays a key role in many DNA transactions, including site-specific recombination, replication and transcription. In most of cells, assemblies of these snups are regulated by DNA architectural proteins which modify the trajectories of DNA segments in a more or less defined way through DNA bending. However, little is known about the external factors such as the morphological state of DNA, which could affect the dynamics of functional snups formation in the genome.

The integration host factor (IHF) is a key DNA architectural protein in *Escherichia* coli [1]. IHF has two homologous subunits, the α- and the β-subunit and it shows limited DNA sequence preference. Both subunits are ~10 kDa and are ~30% identical in sequence. The two subunits are intertwined to form a compact structure, from which two long β ribbon "arms" extend (Fig. 3.1) [2].

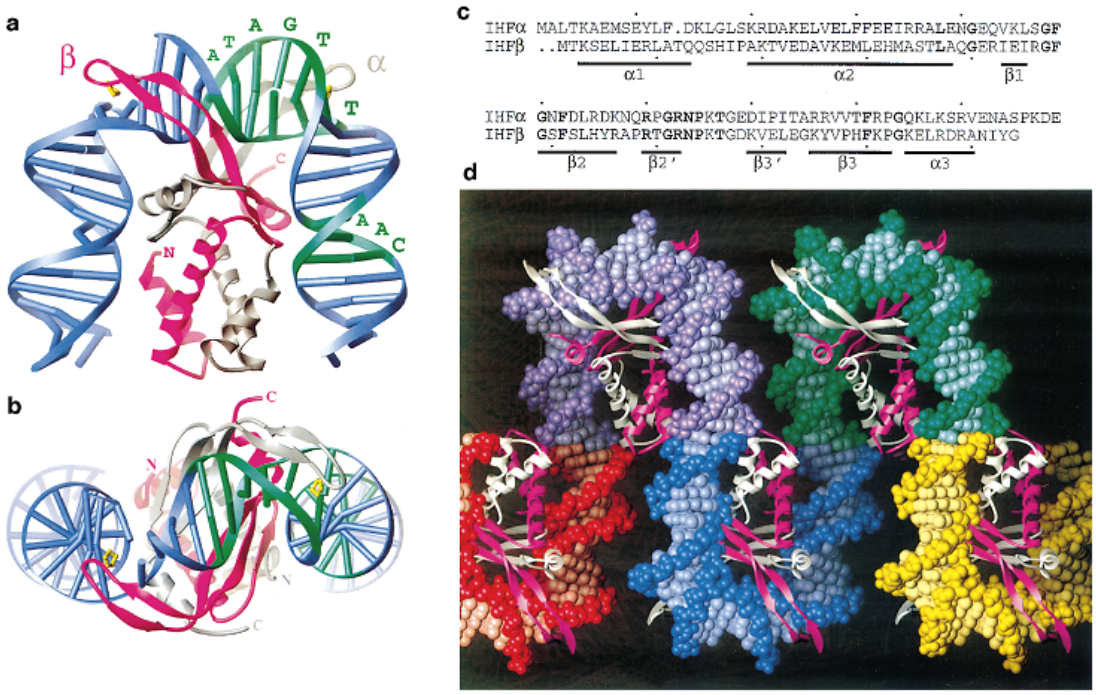

Fig. 3.1 Structure of IHF protein (Picture is copied from Phoebe A. Rice et al [2]).

a) The α - subunit and β - subunit are shown in white and pink, respectively. Double helix DNA is represented in blue and the green part on it is the consensus sequence which interacts mainly with the arm of α – subunit and the body of β – subunit.

b) The top view of IHF – DNA complex.

c) Sequence and secondary structure of the two subunits.

d) The crystal structure of IHF-DNA complexes (5 asymmetric units are shown).

Many works have been done on IHF-DNA snups, including crystal structure of IHF in complex with the phage λ H' site, fluorescent resonance energy transfer (FRET) analyses and visualization of IHF-DNA complexes through atomic force microscopy [2-4]. All of these revealed a strong protein-induced DNA bending (120-160°). The bending is mainly caused by the intercalation of one conserved proline residue from each subunit of heterodimer in to the DNA minor groove. By electrostatic interaction

round the protein body, the DNA U-turn conformation is then stabilized [5, 6].

IHF is involved in the regulation of more than 100 genes in Gram-negative bacteria and it is an essential cofactor in phage λ site-specific recombination, where the protein serves an architectural role during the assembly of snups [7, 8]. Phage attachment (att) site attP, composed of 240 bp, is one of the two recombination sequences in the integrative pathway and harbors three specific IHF-binding sites which must be occupied by IHF to form a functional snup, the so-called integrative intasome. Moreover, negative DNA supercoiling of attP is necessary for intasome assembly [9]. The intasome then captures the protein-free 21 bp attB to form a synaptic complex in which two successive rounds of DNA strand exchange are catalyzed by phage λ integrase (Int).

Our collaborator transferred the phage λ recombination system to mammalian cells and engineered a single-chain IHF, named scIHF2, which is functional in mammalian cells. The scIHF2 differs from wild-type IHF in that almost the entire α-subunit is inserted into the β-subunit at position 39 using two short peptide linkers (Fig. 3.2) [10]. Their biochemical and functional assays confirmed that scIHF2 behaves like its heteromeric parent. A variant of scIHF2, called scIHF2-K45αE was also identified, and it carries glutamate instead of lysine at position 45 of the α-subunit[10]. Besides, one of the two linkers is shortened in scIHF2-K45αE. This new variant is found to be nearly inactive in promoting integrative recombination *in vitro*, while remaining fully active as a co-factor for excisive recombination on supercoiled DNA. The protein also exhibits a defect in its function as an initiation

factor for pSC101 replication *in vivo*.

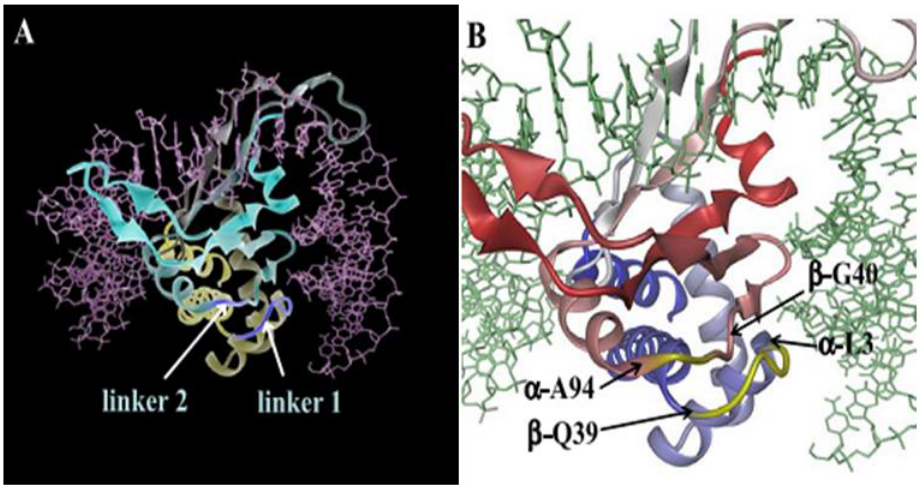

Fig. 3.2 Structure of single-chain IHF (scIHF) [10]

A) ScIHF2-H'structure. The two linkers (labeled 1 and 2) used to connect the two subunits in scIHF2 are highlighted in cyan. The DNA is depicted in purple.

B) Zoomed-in image highlighting the two linkers and the respective residues that were chosen to connect the two IHF subunits

In this research, the interesting phenotype is analyzed in detail by introducing the K45αE substitution into scIHF2. This leads to the identification of a novel, controllable modular mode of protein-induced DNA bending. In addition, the results obtained with the phage λ site-specific recombination system provide valuable insight into possible dynamics of functional snup formation in general, and how this can be governed by an intricate interplay between DNA architectural proteins and external factors.

3.2. Methods

Procedure for APTES functionalization.

99.9% Aminopropyltriethoxysilane (APTES) was diluted 1000x using deionized water and the 0.1% (v/v) APTES was placed on newly stripped mica surface for 15 minutes. After incubation, the APTES solution was removed and the mica was washed with 100 mL deionized water and then dried with steady nitrogen flow. The APTES-treated micas were stored in desiccators for further use.

Procedure for Glutaraldehyde functionalization.

50% Glutaraldehyde was diluted 50 times using deionized water and the 1% (v/v) glutaraldehyde was placed on the APTES-treated mica surface for 15 minutes. After incubation, the glutaraldehyde solution was removed and the mica was washed with 100 mL deionized water and then dried with steady nitrogen flow. The Glu-treated micas were stored in disiccator for 6 hours before use.

AFM imaging of DNA-protein complexes.

Binding reactions contained 0.246 nM attL and a 10, 30 and 100-fold excess of IHF, scIHF2 and scIHF2-K45αE, respectively, in 0.5x TBE buffer, and were incubated at room temperature for 40 minutes. Droplets of 30 μL were spotted onto

APTES-mica or Glu-mica and incubated for 15 minutes. Samples were washed with deionized water and dried under pure nitrogen flow. Imaging was done with a Veeco Dimension 3000 AFM and Nanoscope IIIa controller (Digital Instruments, Santa Barbara, CA, and U.S.A). PPP-NCH silicon tips (NANOSENSORS, Switzerland) were used in tapping-mode scanning (line rate = 1.0 Hz). Images were analyzed with the Nanoscope software and the free software 'ImageJ'.

3.3. Results

A 623 bp attL-carrying DNA fragment was used for AFM imaging. The proteins harbor the H' site positioned asymmetrically 200 bp from one end of DNA. DNA was incubated with different kinds of IHF including wild-type IHF, scIHF2, and scIHF2-K45αE, and then the DNA-protein complexes were absorbed to mica. DNA without protein was used as control (Fig. 3.3). AFM images that showed both a protein signal (a bright dot in the picture) and DNA bending at the expected DNA region were further analyzed (Fig. 3.4，Fig. 3.5，Fig. 3.6).

None of the more than 100 images inspected in the control sample with naked DNA show significant DNA bending together with a protein signal at a corresponding position (Fig. 3.3). Our analysis of AFM images from wild-type IHF-DNA and scIHF2-DNA complexes reveal mean bending angles of 117 (±19) ° and 114 (±15) °, respectively (Fig. 3.4，Fig. 3.5，Fig. 3.6, Fig. 3.7 a and b). The bending angle is defined as the angle that is larger than 90º but less than 180º because the DNA is supposed to

be linear originally. Thus, the bending angle, in most of case, is calculated by subtracting the measured angle from 180º. These values are in very good agreement with those from another AFM study performed with wild-type IHF on a segment from the TOL plasmid[4]. Our analysis using scIHF2-K45αE, however, yields a significantly smaller mean value of 91 (±19) ° degrees (Fig. 3.7 c). Together, these results support our hypothesis that the degree of overall DNA bending in scIHF2-K45αE-DNA complexes is reduced significantly, most likely as a result of weakened protein interaction with the left DNA arm that results from the K45αE substitution. This was proved by crystal structure study of scIHF2 and scIHF2-K45αE in complexes with H' DNA (this part was done by our collaborator).

The AFM images indicate that a scIHF2-K45αE-DNA complex can adopt two stable conformational states. In the "open" state, the left DNA arm is mostly detached from the protein body, thus, leading to a significantly smaller degree of overall DNA bending. In the "closed" state, two divalent metal ions stabilize left arm interactions with the protein body, which results in the more severe DNA bending observed in the crystal structure.

In order to establish that scIHF2-K45αE can also adopt the closed conformational state with covalently closed H'-DNA, scIHF2 and scIHF2-K45αE were incubated with H'-DNA in the presence of magnesium ions, and were analyzed through EMSA (This is done by our collaborator). The results indicated by the change in retardation factor (R_f), small amounts of magnesium ions in the binding and electrophoresis buffer almost completely reversed the supershift of the scIHF2-K45αE-H' complex

relative to that of scIHF2-H' analyzed under the same condition.

To make statistical analysis, we performed AFM experiment with attL in the presence of nanomolar to micromolar concentrations of metal ions was repeated so as to obtain further evidence that the presence of magnesium ions induces the formation of a closed conformational state between scIHF2-K45αE and an intact cognate site. We found that, under these conditions, the DNA bending obtained with scIHF2-K45αE increased to the values observed with scIHF2. In the 200 nM or 20 nM Mg^{2+}, the mean bending angles in the scIHF2-K45αE protein condition were 114 (±15) ° and 111(±22) ° (Fig. 3.8, Fig. 3.9, Fig. 3.10), respectively.

All these results indicate that a nicked DNA backbone is not prerequisite for the formation of the closed conformational state in a scIHF2-K45αE-DNA complex. In addition, this finding raised the interesting possibility of modulating the activity of scIHF2-K45αE in recombination reaction through a metal ion-mediated increase in DNA bending. As shown in Fig. 3.8-b, a small amount (20nM) of magnesium ions does affect the activity of scIHF2-K45αE in integrative recombination.

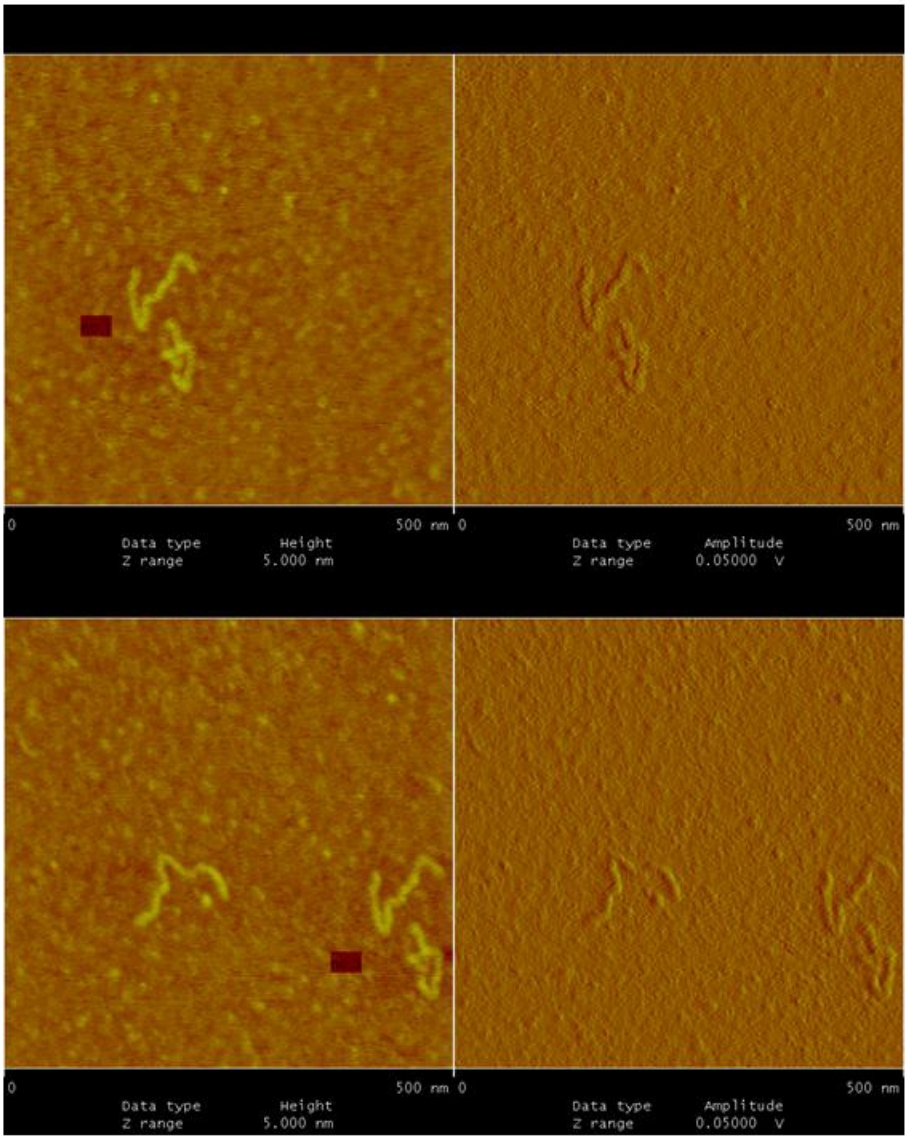

Fig. 3.3 AFM images of attL DNA on mica surface

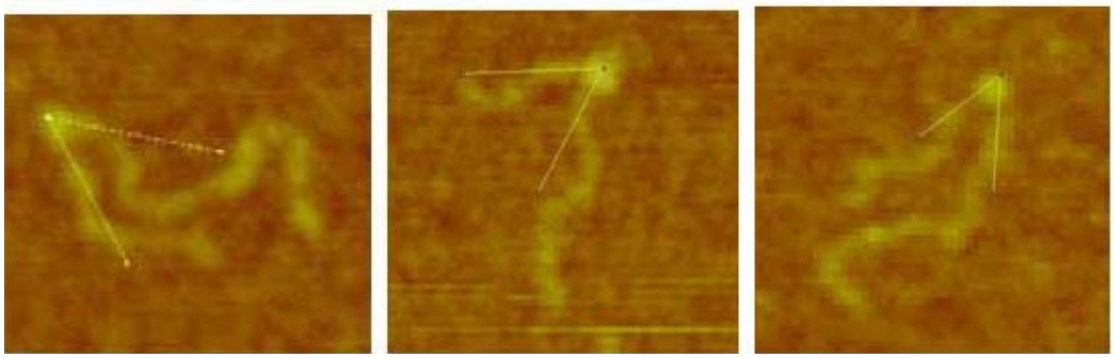

Fig. 3.4 Zoom-in images of wild-type IHF induced DNA bending. (The bright dot in the 2/3

part of DNA indicates a wild-type IHF in the expected location)

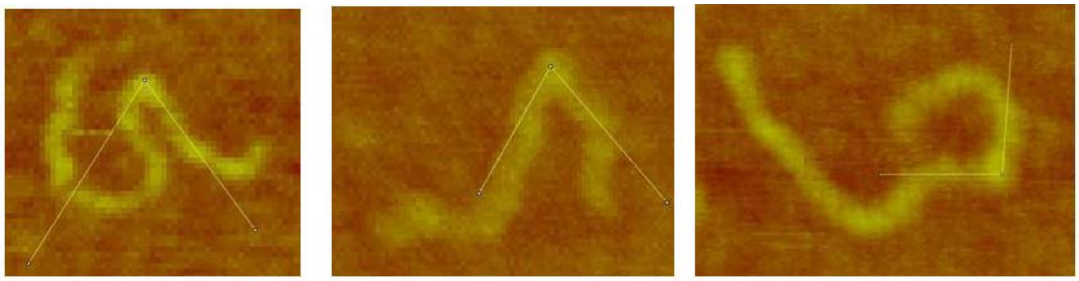

Fig. 3.5 Zoom-in images of scIHF2 induced DNA bending. (The bright dot in the 2/3 part of DNA indicates a scIHF in the expected location).

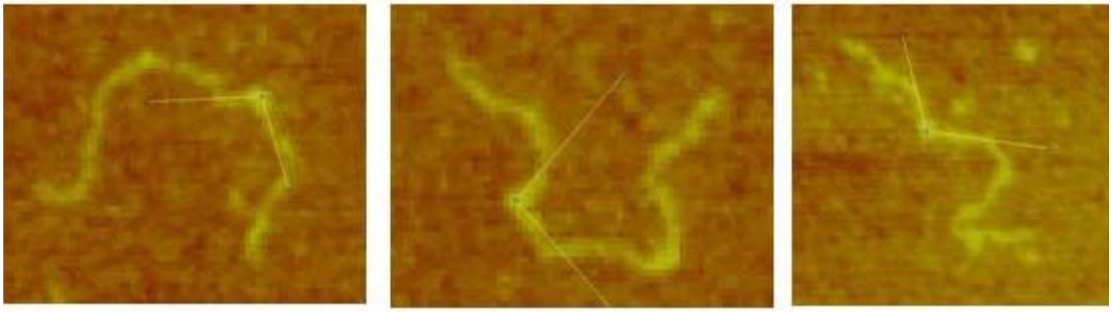

Fig. 3.6 Zoom-in images of scIHF2-K45αE induced DNA bending. (The bright dot in the 2/3 part of DNA indicates a scIHF2-K45αE in the expected location).

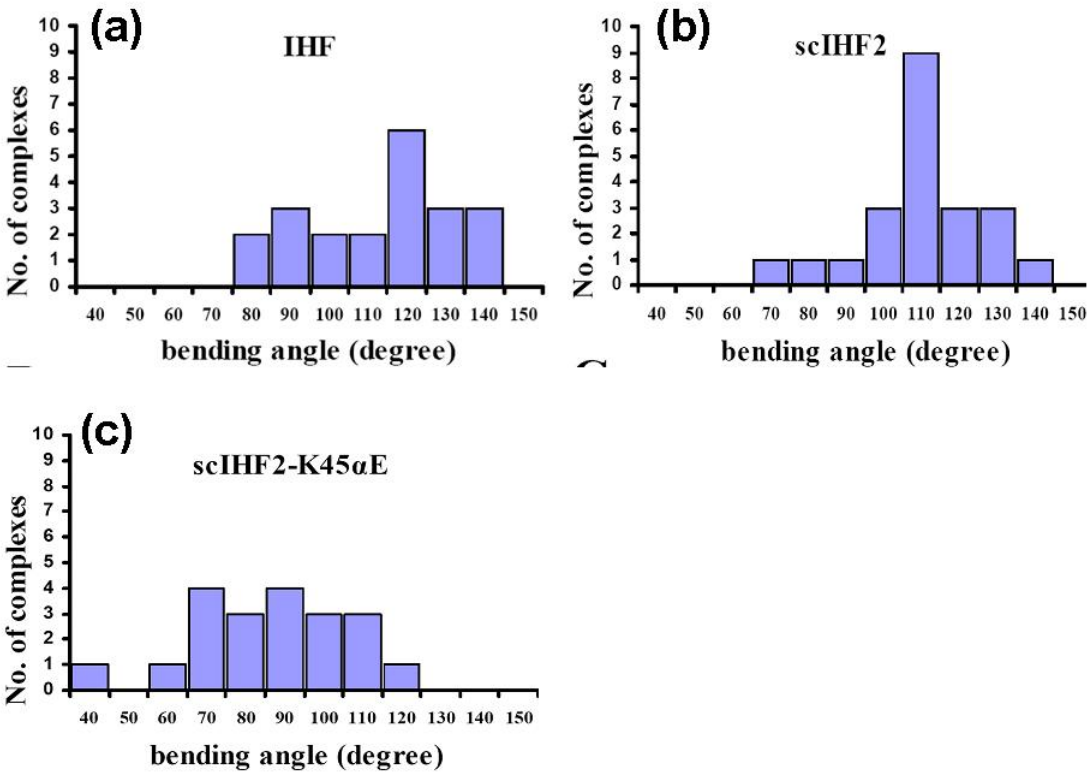

Fig. 3.7 Histogram of bending angle distribution.

a) Bending angle distribution of wild-type IHF; Mean bending angle is 117(±19º).

b) Bending angle distribution of scIHF2; Mean bending angle is 114(±15º).

c) Bending angle distribution of scIHF2-K45αE; Mean bending angle is 91(±19º).

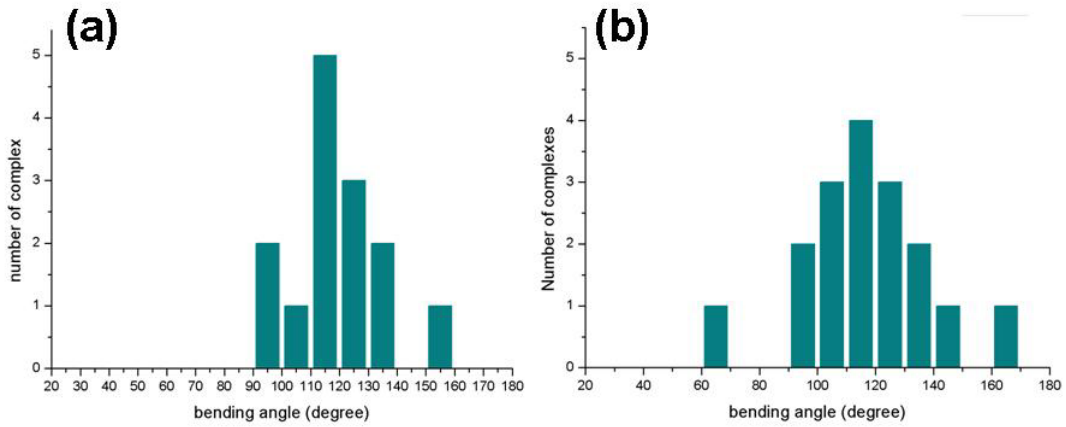

Fig. 3.8 Histogram of bending angle distribution of Mg^{2+} dependence

a) Bending angle distribution of scIHF2-K45αE in 200 nM Mg^{2+} solution; Mean bending angle is 120 (±17 º).

b) Bending angle distribution of scIHF2-K45αE in 20 nM Mg^{2+} solution; Mean bending angle is 117.5 (±21 º).

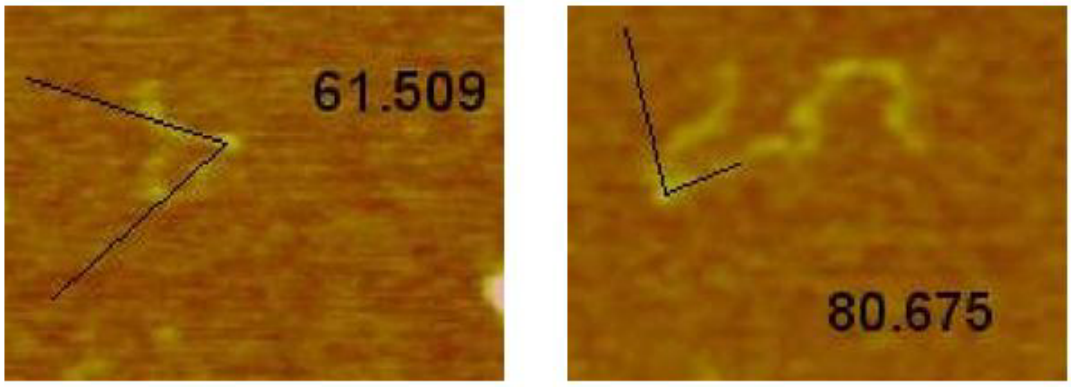

Fig. 3.9 Zoom – in image of scIHF2-K45αE induced DNA bending in 20 nM Mg^{2+} solution condition (the bright dot in the 2/3 part of DNA indicates a scIHF2-K45αE in the expected location)

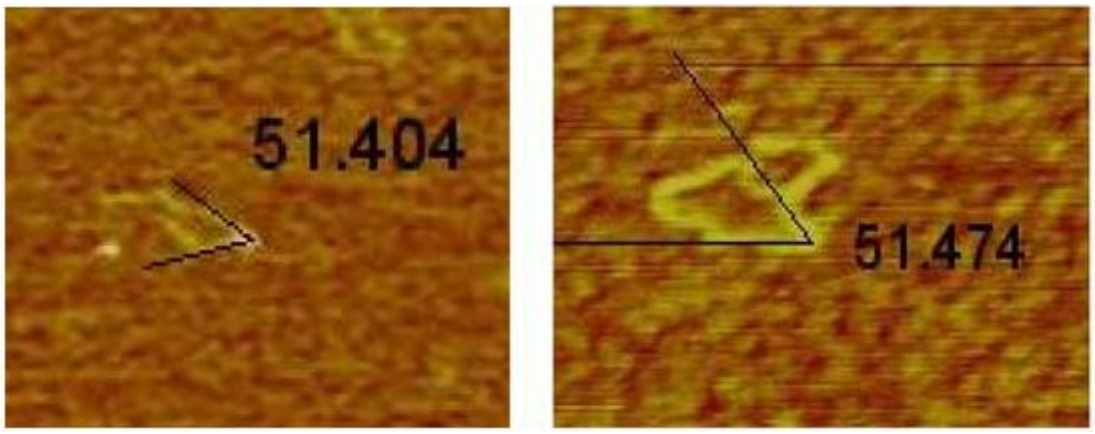

Fig. 3.10 Zoom – in image of scIHF2-K45αE induced DNA bending in 200 nM Mg^{2+} solution condition (the bright dot in the 2/3 part of DNA indicates a scIHF2-K45αE in the expected location)

3.4. Discussion

The regulational mode of DNA bending by scIHF2-K45αE can be exploited to study the topography of snups. This is exemplified by the assembly of λ intasomes, which is required for synapsis of att sites and for subsequent progression through the entire recombination reaction. The paths of the recombining DNA substrates differ in shape in intasomes configured for integration versus excision. A number of studies in which IHF was replaced by other architectural proteins or sequence-directed bends already confirmed important intasomal DNA architectural requirements [9, 11, 12].

The functionally important cognate site for IHF in attR is H2. It is located in close proximity to the two target sites for the second DNA-bending factor, Xis. Earlier reports identified the attR intasome as a more delicate structure than the attL intasome, and an inspection of recent modeling of the DNA path in the attR intasome clearly predicted a need for extreme DNA-bending at H2. Our result strongly support this model and reveals that an open scIHF2-K45αE-H2 conformation on attL, with overall DNA bending angles significantly smaller than those found in complexes with scIHF2 or wildtype IHF, is not functional. In this case, DNA supercoiling is most likely required to overcome a thermodynamic barrier imposed on the formation of a stable closed scIHF2-K45αE-H2 complex, arising from the combined effects of the stiffness of short DNA segments and weakened interaction between the left DNA arm and the protein body of scIHF2-K45αE.

The fact that IHF and scIHF2 activate recombination on topologically relaxed attR indicates that wild-type IHF-DNA interactions are sufficiently strong in the

absence of supercoiling. However, there appears to be no strict requirement for severe IHF-induced bending inside the attL intasome, where open scIHF2-K45αE-H' complex seems sufficient to configure a functional snup.

Our results also provide insight into snup formation during integrative recombination. Our finding that scIHF2-K45αE is barely active in integrative recombination, but is significantly stimulated by divalent metal ions, indicates that a closed scIHF2-K45αE-DNA complex with a high degree of DNA bending must be a prerequisite to permit necessary Int-DNA interactions with attP. Integrative and excisive recombination differ most notably in their requirement for the IHF cognate site H1 and, again, inspection of recent models for integrative intasomes indicates that a closed scIHF2-K45αE-DNA complex is most likely required there. In addition to the proposed effect on the degree of bending at H1 by scIHF2-K45αE-DNA, a more complex dependence involving cooperative protein binding effects, including the two other IHF binding sites, is possible.

ScIHF2-K45αE-DNA may be a valuable tool to investigate nucleoprotein complex formation in general. It could be used to probe the topography of specific snups involved in DNA transactions *in vitro* and *in vivo*, in both prokaryotic and eukaryotic cells. An interesting feature application could include the generation of *E.coli* strains that express either scIHF2 or scIHF2-K45αE instead of wild-type IHF, and perform comparative gene expression profiling in order to probe the topography of IHF-dependent snups involved in gene regulation.

Engineering of metal-binding sites at the IHF-DNA interface holds promise for

the design of switches in other DNA-binding systems. As we have applied the scIHF2 variant in this study, DNA binding or conformational alteration that is dependent on divalent metal concentration can be exploited for probing structure-function relationship in other nucleoprotein assemblies. It would be informative to investigate the general effect of substituting basic amino acid residues that are involved in phosphate group contacts with acidic residues in other DNA-binding proteins. Our results suggest such changes may give rise to a requirement for a divalent metal-meditated protein-DNA interaction for stabilizing the native-like, DNA-bound configuration. Such metal-dependent modulation could be exploited for the design of nano-sized DNA switch devices.

3.5. References

[1] J. A.Goodrich, M. L.Schwartz, and W. R.McClure, Nucleic Acids Research **18**, 4993 (1990).

[2] P. A. Rice, S.-w. Yang, K. Mizuuchi, and H. A. Nash, Cell **87**, 1295 (1996).

[3] M. Lorenz, A. Hillisch, S. D.Goodman, and S. Diekmann, Nucleic Acids Research **27**, 4619 (1999).

[4] G. H. Seong, E. Kobatake, K. Miura, A. Nakazawa, and M. Aizawa, Biochemical and Biophysical Research Communications **291**, 361 (2002).

[5] T. Ellenberger, and A. Landy, Structure **5**, 153 (1997).

[6] K. K. Swinger, and P. A. Rice, Current Opinion in Structural Biology **14**, 28 (2004).

[7] S. M. Arfin, A. D. Long, E. T. Ito, L. Tolleri, M. M. Riehle, E. S. Paeglei, and G. W. Hatfield, Journal of biological chemistry **275**, 29672 (2000).

[8] M. W. Mangan, S. Lucchini, V. Danino, T. Ó. Cróinín, J. C. D. Hinton, and C. J. Dorman, Molecular Microbiology **59**, 1831 (2006).

[9] E. Richet, P. Abcarian, and H. A. Nash, Cell **46**, 1011 (1986).

[10] Q. Bao, N. Christ, and P. Droge, gene **343**, 99 (2004).

[11] C. A. Davey, D. F. Sargent, K. Luger, A. W. Maeder, and T. J. Richmond, Journal of molecular biology **319**, 1097 (2002).

[12] S. D. Goodman, and O. Kay, The journal of biological chemistry **274**, 37004 (1999).

Chapter 4. Single DNA study of VP15-DNA interaction

4.1. Introduction

Chromosome DNA in most eukaryotic cells is compacted into nucleosome-based chromatin. However in some eukaryotes, prokaryotes, and viruses, DNA compaction is not based on formation of nucleosomes. For instance, in bacteria, the compaction is contributed mostly from DNA bending or bridging proteins[1].

In viruses containing a DNA genome, the compaction is achieved mostly by interaction between DNA and capsid proteins [2-5]. Compared to the understanding of how DNA is packaged in eukaryotes and in bacteria, DNA packaging by capsid proteins in viruses is much less understood.

Discovered in South Asia at the beginning of the 1990s, the white spot syndrome virus (WSSV) has brought a devastating epidemic to the shrimp industry. It belongs to the virus family Nimaviridae, genus *Whispovirus* [6] and has a circular double-stranded DNA (dsDNA) genome of around 300 kbp. Many researches have focused on the structural proteins of WSSV and nine major nucleocapsid structural proteins were identified previously [7, 8]. Among them, VP15 is a highly basic protein located in the nucleocapsid with a theoretical molecular weight of 6.7 kDa and a pI of 13.2 [9]. Such a high pI suggests that it may be a DNA binding protein and therefore may play an important role in packaging DNA into the nucleocapsid. Earlier studies suggest that VP15 binding to DNA was based on electrophoretic mobility shift

assay (EMSA) [9, 10]. More recent studies showed that VP15 can interact with itself to form homomultimers, but not with the other major structural proteins of WSSV [9]. Although these results suggest that VP15 may play a role in packaging the WSSV genome into the nucleocapsid, it remains unclear how VP15 interacts with dsDNA to achieve the packaging. This study aims to investigate the details of interaction between VP15 and dsDNA. We expect the knowledge obtained in the research will be useful in understanding dsDNA packaging in WSSV, and more generally shed light on how capsid proteins of DNA viruses interact with the viral genomes.

In contrast to the earlier experiments which were based on bulk information, our studies are mainly based on the recently developed single-molecule manipulation, which allows us to directly observe the dynamical process of DNA packaging at the single-DNA level, and to image individual DNA package. We studied the DNA compaction against controlled tensional force using a transverse magnetic tweezer ssetup (MT) described by J.Yan et al [11], and we imaged the conformations of the VP15-DNA complexes using atomic force microscopy (AFM).

4.2. Methods

Electrophoretic mobility shift assay (EMSA)

50 ng DNA (linearized Phix174 of 5386 bp) was mixed with purified VP15 at different ratios to a final volume of 20 ul in PBS buffer (137 mM Sodium Chloride, 2.7 mM Potassium Chloride, 10 mM Phosphate Buffer, pH 7.3). The mixture was

incubated at room temperature for 30 minutes. The DNA-binding capacity of VP15 was examined in 1% agarose gels in TBE buffer (89 mM Tris, 89 mM Borate, 2 mM EDTA, pH 8.25). The DNA was visualized under UV light after being stained using ethidium bromide for 30 minutes.

Magnetic-tweezer Manipulation of VP15-DNA complex

The two ends of the 48.5kbp λ-DNA molecules were labeled using biotin and digoxygenin oligonucleotides, respectively [12]. One end of a labeled DNA was then bound to a 2.8-micron-diameter paramagnetic bead, and the other end to an edge of a thin $0^{\#}$ cover glass which is coated with anti-digoxygenin. A permanent magnet was placed outside the channel, responsible in generating controlled forces up to 50 pN to the bead. The system is illustrated in chapter II. The forces were applied on the focal plane of the objective, and the extension of DNA was determined by measuring the distance between the bead and the edge of the cover glass along the force direction. The forces were measured by using bead thermal motion [13]. Our setup is an improved version of the 'transverse MT' [11] which was used to study Fis-DNA interaction [14] and chromatin assembly in Xenopus egg extracts [15]. Before addition of the protein, the force-extension curve of the dsDNA was measured and the persistence length value (represented by "A") was obtained by fitting the Marko-Siggia formula [16] for forces (F) from 0.5 pN up to 10 pN. The tether between the glass edge and the paramagnetic bead DNA is determined to be a single

DNA if the value of A is 50 ± 3 nm, which was known to be in the range of DNA persistence length under usual physiological buffer conditions. After force calibration, VP15 was diluted in PBS and injected into the flow cell, and the extension of DNA under different forces was recorded in real time. All experiments were conducted at room temperature.

Atomic Force Microscopy imaging of VP15-DNA complex

The complexes of VP15 and DNA were formed by incubating 10 ng of Phix174 DNA with different concentrations of VP15 in PBS solution for 20 minutes at room temperature. This mixture was then deposited onto the glutaraldehyde-treated mica for another 10 minutes at room temperature. These mica disks were then gently rinsed with distilled water, and dried by a steady stream of nitrogen. Images were acquired using Agilent PicoPlus, operating in tapping mode in air with silicon AFM probe.

4.3. Results

EMSA experiment confirmed that VP15 is a DNA-binding protein and it can package DNA cooperatively when the protein concentration exceeds a threshold value.

As a comparison with the EMSA results reported by Witteveldt *et al* [9] and Zhang et al [10], we performed similar EMSA experiments to study how VP15 affects the mobility of 5386 bp linearized Phix174 DNA.

The mobility of the DNA is not considerably affected at up to 165 nM concentrations of VP15 (Fig. 4.1). A dramatic change in the mobility started at the concentration of 330 nM, at which two separating DNA bands were found, indicating coexistence of two conformational states of the DNA molecules. The smeared frontier moved almost as fast as the naked DNA, suggesting weak changes in the conformation of the DNA and the charge-distribution on the DNA. The other band moved extremely slowly, only barely entered the gel, indicating a dramatic change to the DNA conformation.

At even higher concentrations (1650 nM and 3300 nM), the fast moving band disappeared because all DNA was stacked in the well. At an ultra high concentration (6600 nM), the DNA could hardly penetrate into the gel.

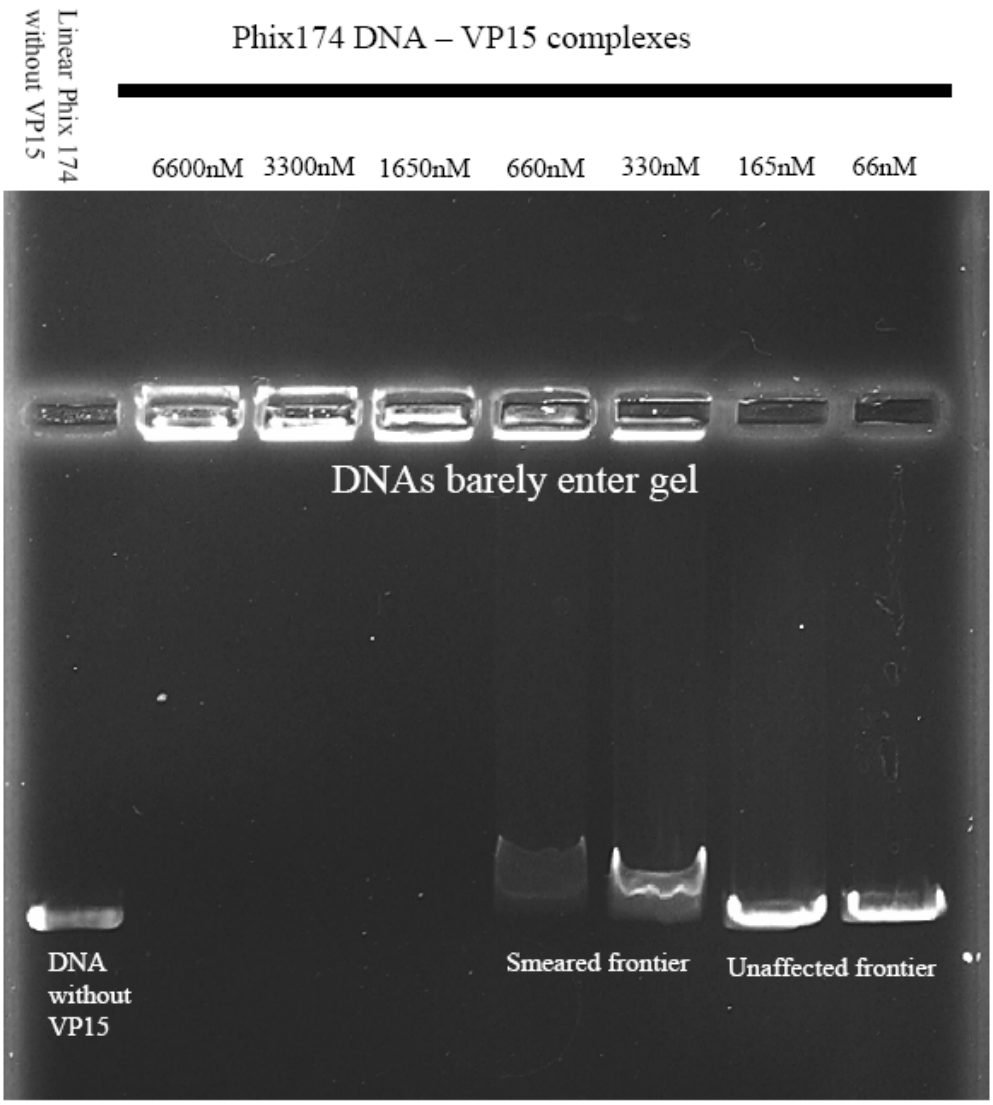

Fig. 4.1 Electrophoretic mobility shift assay (EMSA).

(70 ng of linear Φ174 DNA was incubated with different concentrations of VP15 for 30 min at room temperature and then analyzed in 1% agarose gel. Obvious shift was observed when the concentration of VP15 was above 330 nM.)

Magnetic tweezer (MT) experiments revealed that VP15 could compact DNA against certain forces when the protein concentration was larger than a threshold value.

In our MT experiments, considerable DNA compaction was not observed at VP15 concentrations lower than 6.6 nM in the force range (> 0.2 pN). When the concentration is larger than 6.6 nM, the critical force that could stop the folding was found to be dependent on the protein concentration: the higher the concentration, the larger the critical force.

Fig. 4.2 a and b show DNA compaction at 33 nM and 66 nM respectively and a complicated folding behavior was observed. An increase in the concentration by two times resulted in a dramatic increase in the overall folding rate by more than 10 times even at a high force. Under these concentrations, the folding time courses did not show stepwise signals, and the folding rate varied in a wide range, indicating that folding was not caused by formation of any simple regular local structures. This is in contrast to the formation of nucleosomes in chromatin assembly [15] and formation of DNA toroids by multivalent cations [17], where regular stepwise folding and unwinding dynamics were reported in magnetic tweezer or optical tweezer experiments.

The 6.6 nM VP15 concentration was found to be a critical concentration. Fig. 4.2. c and d show two experiments at 6.6 nM. In Fig. 4.2 c, intermittent large scale folding and unfolding fluctuations were observed at a constant force of 1.3 pN with magnitudes ranging from 200 nm to a few micrometers. The observation of both the

folding and unfolding at the same force with similar magnitudes suggests that the concentration of 6.6 nM is close to the threshold value. Fig. 4.2 d shows another experiment conducted at the same concentration. Again, similar fluctuations were observed at 1.24 pN, 0.55 pN, and 0.22 pN. Considerable DNA compaction was not observed at concentrations less than 6.6 nM in the force range larger than 0.2pN. Therefore, we conclude that 6.6 nM is close to a minimal concentration that is required for DNA packaging by VP15.

Fig. 4.3 a and b show the unfolding dynamics under large forces. The DNA folded in 6.6 nM VP15 solution could be nearly fully unfolded under ~3 pN (Fig. 4.3 a). The unfolding was intermittent, suggesting the existence of energy barriers which are needed to be overcome in the unfolding pathway. The DNA folded in 66 nM VP15 required larger force for unfolding. Fig. 4.3 b shows that even the force of 13 pN could not completely unfold the DNA in 20 minutes. In addition, unlike the intermittent unfolding observed in 6.6 nM VP15, the unfolding in 66 nM VP15 was not apparently intermittent. We noticed that the folding and unfolding dynamics are intermittent at 6.6 nM, while they are not at 66 nM.

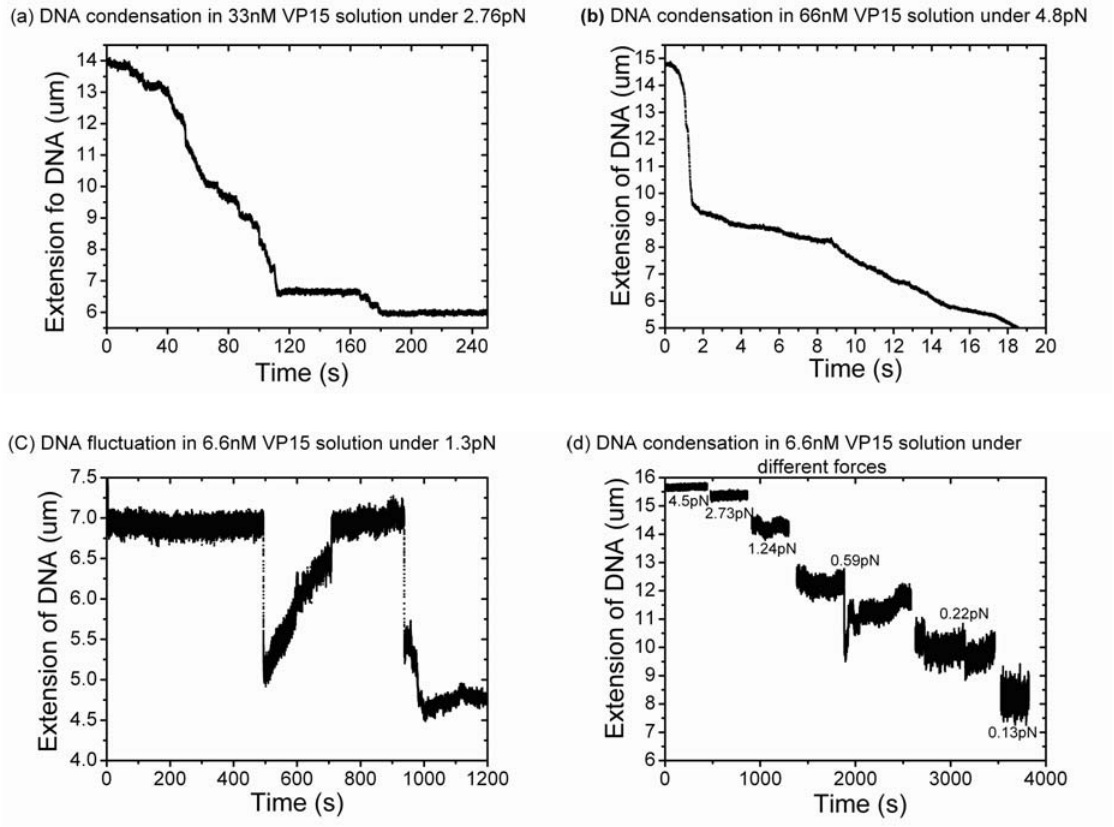

Fig. 4.2 DNA folding dynamics under different forces and different VP15 concentrations.

a) DNA dynamical process under 2.76 pN in 33 nM.

b) DNA dynamical process under 4.8 pN in 66 nM.

c) DNA dynamical process under 1.3 pN in 6.6 nM. Both folding and unfolding were observed.

d) DNA dynamical process under different forces in 6.6 nM. DNA folding/unfolding fluctuations were revealed under 1.24 pN, 0.59 pN, and 0.22 pN.

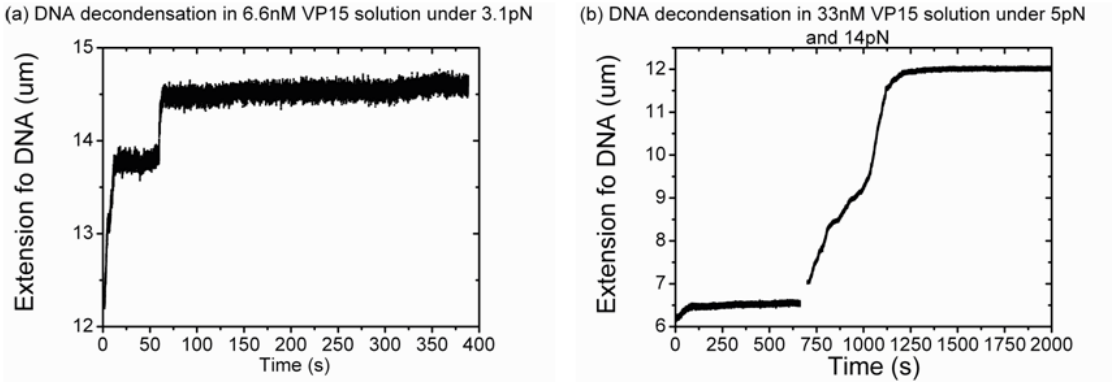

Fig. 4.3 DNA unfolding dynamics under different forces and different VP15 concentrations.

a) DNA dynamical process under 3.1 pN in 6.6 nM. Intermittent unfolding events were observed.

b) DNA dynamical process under 5 pN (0 – 600 Sec) and 14 pN (670 – 2000 Sec) in 33 nM. Unfolding is not intermittent.

AFM experiments revealed that VP15 packages DNA by making synergies between remote DNA sites.

Fig. 4.4 shows AFM images of DNA-VP15 complexes at different VP15 concentrations. At 0.66 nM (Fig. 4.4 b), DNAs were mostly free of proteins, while at 66 nM (Fig. 4.4 c-e), mild local folding started as rarely distributed hairpin structures (Fig. 4.4 c), bridging of remote DNA sites forming large DNA loops (Fig. 4.4 d), and bridging many DNA together, forming a flower-like structure with protein-rich center and protein-free DNA surrounding the center (Fig. 4.4 e). At this concentration, a large portion of DNA backbone was unbound by VP15. When the concentration of VP15 was increased to 660 nM, the DNA was compacted into tightly folded DNA bundles (Fig. 4.4 f).

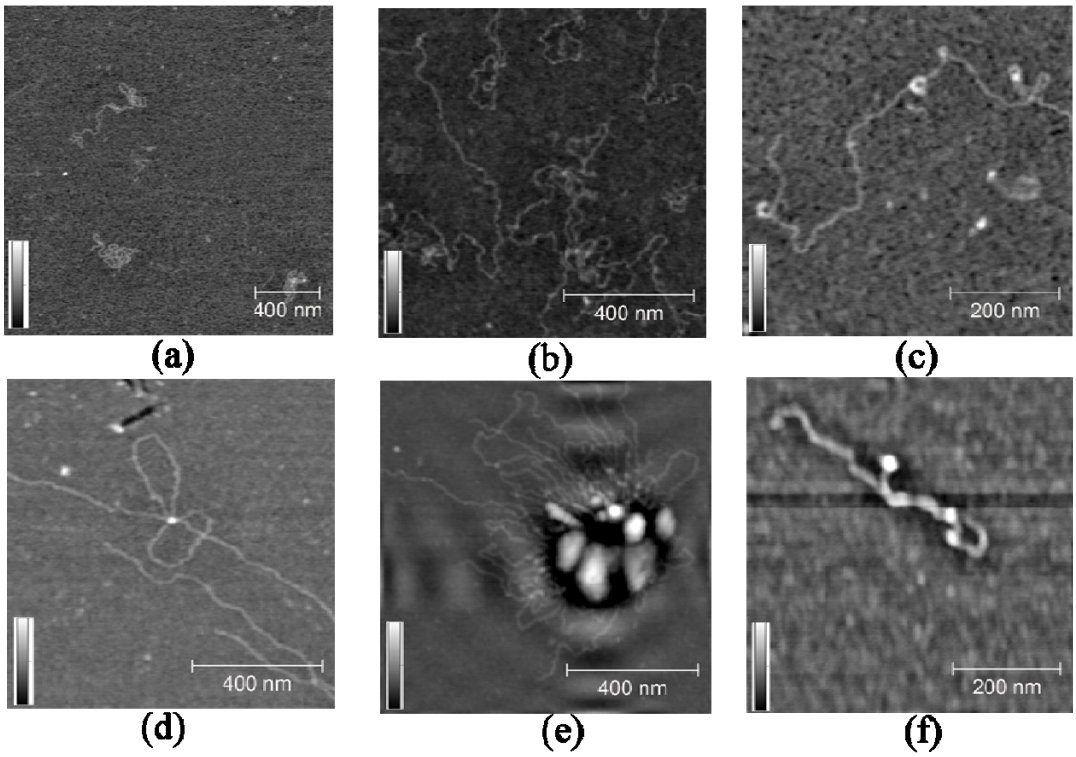

Fig. 4.4 AFM images of linear phix174 DNA with and without VP15. (The height scale bar ranges from 0 – 2nm for Fig. 4.4 a - d and f, and from 3 – 8nm for e)

a) DNA molecules without VP15 on a 2 μm x 2μm area.

b) DNA molecules after incubation with 0.66 nM VP15.

c - e) DNA molecules after incubation with 66 nM VP15.

f) DNA molecules after incubation with 660 nM VP15.

4.4. Discussion

All the experiments described in the previous sections suggest that VP15 can compact DNA nonspecifically. The dramatic changes in DNA electrophoretic mobility implied dramatic changes in conformations of DNA. The MT experiments confirmed at a single-molecule level that the DNA was compacted by VP15 against forces of a few pN. The AFM experiments further showed that the DNA molecules were folded

into various structures by bringing remote DNA sites together. VP15 tends to stay together on DNA templates (for example, as shown in Fig. 4.4 e), indicating a cooperative binding on DNA.

The packaging mechanism of VP15 is very different from the nucleosome-based DNA packaging in eukaryotic cells, where DNA compaction is dominated by the formation of nucleosomes. It is also different from DNA folding by spermdines and multivalent cations where DNA is often folded into ordered structures of toroids [18]. To a certain extent, it resembles DNA packaging in bacteria, where the DNA compaction is more likely being dominated by DNA bridging proteins [1]. A prominent example is the H-NS proteins which exist as dimers, hence are able to interact with two DNA sites, leading to the formation of large scale hairpin structures [1]. Another prominent example is the Fis proteins which is also able to bring remote DNA sites together and collapse DNA [14]. Although the details of how VP15 proteins form DNA synergies remain unclear, it is likely that they form synergies by VP15-VP15 interaction since it is known that VP15 proteins can form homomultimers [9].

The all-or-none behavior observed in EMSA experiments, the existence of the critical concentration in all the three types of experiments, the abrupt compaction dynamics observed in MT experiments, and the protein localization observed in AFM imaging experiments all suggest a cooperative compaction mechanism. The cooperativity can be easily understood by the fact that VP15 protein can form DNA synergies: subsequent binding of VP15 after a pre-existing synergy is more

energetically favored since it does not require bringing together remote DNA sites that are initially far away from each other. Therefore, the fork of a pre-existing synergy or hairpin becomes a hotspot that invites more VP15 to bind, leading to the cooperative binding behavior. Alternatively, the cooperativity may be explained by direct VP15-VP15 interactions on DNA template. It has been known that VP15 can form homomultimers at high concentrations in solution. At a moderate VP15 concentration, due to the attractive electrostatic interaction with VP15, a DNA may serve as a template around which the local concentration of VP15 may be increased to a level that could promote oligomerization of VP15 and result in the cooperativity.

The existence of a critical concentration c* required for DNA compaction is suggested by all the three different types of experiments. The EMSA experiment suggests a value around 330 nM, the AFM imaging experiment suggests a value around 66 nM, and the MT experiment suggests a value around 6.6 nM. The EMSA and AFM are experiments in bulk. At their respective critical concentrations, the ratios of available proteins per DNA base pair were computed to be ~0.1/bp for the EMSA experiment and ~0.4/bp for the AFM experiment. This suggests that the cooperative folding of DNA likely requires about 1 or more VP15 monomer per 10 bp DNA in a bulk experiment. In the MT experiment, there is only one or very few DNA in the whole reaction volume, so that the free protein concentration is not perturbed by the presence of DNA. Therefore c*=6.6 nM determined in MT experiments is the critical concentration of the free protein in solution required to compact the DNA.

In the MT experiments, when the protein concentration *c* is larger than or equal to

the critical concentration c^*=6.6 nM, it was found that the DNA compaction could start only when the tension f is smaller than a certain critical value f^*. This critical force f^* was found to be dependent on the protein concentration: a larger c led to a larger f^*. A plausible explanation to this concentration dependent critical force is that to initiate the cooperative DNA compaction process, an initiating DNA loop must be formed and mediated by VP15-VP15 interactions. Therefore, the balance between the DNA looping free energy in the presence of a force and the protein binding free energy eventually leads to the concentration-dependent critical force, as originally shown in [14].

In summary, we have shown that the capsid protein VP15 can bind and fold DNA into various structures by forming synergies between remote DNA sites. Its binding is cooperative, and the resulted folding is capable of withstanding forces of a few pico Newtons. It has been shown that the mechanism of cellular DNA compaction includes bending, wrapping and bridging of DNA by architectural proteins [19]. However, the underlying mechanisms for viral genome compaction are poorly studied. Our research is the first study to reveal the binding affinity and dynamical process of VP15 condensation using single DNA manipulation. It sheds light on the strength of the compact capability of VP15 and may represent a new mechanism of viral genomic compaction.

4.5. References

[1] R. T. Dame, Molecular Microbiology **56**, 858 (2005).

[2] M. V. Borca, P. M. Irusta, G. F. Kutish, C. Carrillo, C. L. Afonso, T. Burrage, J. G. Neilan, and D. L. Rock, Archives of Virology **141**, 301 (1996).

[3] G. Krishnamoorthy, B. Roques, J.-L. Darlix, and Y. M. Â. ly, Nucleic Acids Research **31**, 5425 (2003).

[4] M. S. Luijsterburg, M. F. White, R. v. Driel, and R. T. Dame, Critical Reviews in Biochemistry and Molecular Biology **43**, 393 (2008).

[5] S. Sun, K. Kondabagil, B. Draper, T. I. Alam, V. D. Bowman, Z. Zhang, S. Hegde, A. Fokine, M. G. Rossmann, and V. B. Rao, Cell **135**, 1251 (2008).

[6] M.A.Mayo, Archives of Virology **147**, 1655 (2002).

[7] Z. Li, Q. Lin, J. Chen, J. L. Wu, T. K. Lim, S. S. Loh, X. Tang, and C.-L. Hew, Molecular & Cellular Proteomics **6**, 1609 (2007).

[8] M. C. W. v. Hulten, M. Reijns, A. M. G. Vermeesch, F. Zandbergen, and J. M. Vlak, Journal of General Virology **83**, 257 (2002).

[9] J.Witteveldt, A. M. G. Vermeesch, M. Langenhof, A. d. Lang, J. M. Vlak, and M. C. W. v. Hulten, Archives of Virology **150**, 1121 (2005).

[10] X. Zhang, X. Xu, and C. L. Hew, Virus Research **79**, 137 (2001).

[11] J. Yan, D. Skoko, and J. F. Marko, Physical Review E **70**, 011905 (2004).

[12] S. Smith, L. Finzi, and C. Bustamante, Science **258**, 1122 (1992).

[13] T. R. Strick, J.-F. Allemand, D. Bensimon, A. Bensimon, and V. Croquette, Science **271**, 1835 (1996).

[14] D. Skoko, J. Yan, R. C. Johnson, and J. Marko, Physical Review Letters **95**, 208101 (2005).

[15] J. Yan, T. J. Maresca, D. Skoko, C. D. Adams, B. Xiao, M. O. Christensen, R. Heald, and J. F. Marko, Molecular Biology of the Cell **18**, 464 (2007).

[16] J. F. Marko, and E. D. Siggia, Macromolecules **28**, 8759 (1995).

[17] W.-B. Fu, X.-L. Wang, X.-H. Zhang, S.-Y. Ran, J. Yan, and M. Li, Journal of the American Chemical Society **128**, 15040 (2006).

[18] N. V. Hud, and K. H. Downing, PNAS **98**, 14925 (2001).

[19] M. S. Luijsterburg, M. C. Nooma, G. J. L. Wuite, and R. T. Dame, Journal of Structural Biology **156**, 262 (2006).

Chapter 5. Single DNA study of H-NS-DNA interaction

5.1. Introduction

H-NS is a small (15.5k Da) protein, which can harbor many patches of charged amino acid but shows a neutral pI. It has 137 amino acids in length and has three structural components: An N-terminal domain (residues 1-64) that contains oligomerization activity; a carboxy-terminal domain (C-terminal domain, residues 90-136) that have nucleic-acid-binding activity; and a flexible linker that connects the two [1]. H-NS is present at around 20,000 copies per cell and binds to A-T rich DNA preferentially [2-6]. It exists as a dimer and has the ability to self-associate [7], forming higher order oligomers [8]. The C-terminal domain binds DNA, while the N-terminus is involved in dimerization [9].

H-NS has two different biological functions. Firstly, it plays an important role in the compaction of the nucleoid [10, 11]. Secondly, H-NS also serves an important function in DNA silencing [12], and these two functions may not be mutually exclusive. Recent studies have proposed a unique role of H-NS in keeping horizontally-acquired genes in pathogens switched off until conditions are right for expression of virulence [3, 4, 13]. Thus, H-NS serves as an “immune sentinel”, preventing foreign genes from being deleted from their host. Understanding the role of H-NS in silencing and the mechanisms that relieve silencing has been a major

focus of recent studies, but is limited by the tools available [14-16]. A long-held view is that these dual roles (i.e., DNA compaction and gene silencing) of H-NS are a function of its structural and mechanical modifications to DNA upon binding. It was previously reported using atomic force microscopy imaging (AFM), that H-NS binding led to formation of DNA bridges, i.e., two DNA segments were linked to each other in parallel form [17]. More recently, two parallel, stretched λ-DNA molecules were held close to each other by four laser traps in the presence of H-NS, revealing H-NS-mediated interaction between adjacent DNA strands [18]. These experiments convincingly showed that H-NS could link remote DNA sites together, and promote the formation of DNA bridges. Hereafter, we refer to this binding as the "bridging mode".

A controversy resulted from a single-molecule manipulation experiment using magnetic tweezers was reported by Amit et al [19]. In their experiment, DNA bridging behavior was not observed over a wide protein concentration range and a wide range of forces. Instead, it was showed that during H-NS binding, the DNA adopted a more extended and stiffer configuration compared to naked DNA substrates. This result was in sharp contrast to the previously observed bridging mode, and to date there has been no clear explanation for the difference between these two research findings. Hereafter, we refer to this binding as the "stiffening mode".

Efforts to resolve the discrepancy were unsuccessful [19-21]. It was suggested that the differences were due to the type of measurements being made, e.g., single-molecule measurements compared to bulk measurements [20]. However, this explanation

cannot account for the discrepancy, since the bridging mode of binding was observed in both AFM imaging [17] and later in single-molecule manipulation measurements [18]. Another possibility was that it resulted from the difference between two-dimensional surface imaging measurements and three-dimensional solution measurements [19]. However, this does not resolve the problem either since stiffening was observed in the magnetic tweezer experiment [19], while bridging was also recently observed in an optical tweezer measurement [18], both being in solution condition.

In this study, we resolve these discrepancies using magnetic tweezers and AFM imaging methods. Herein, we report that the switch between the two binding modes of H-NS is mediated by switching the magnesium concentration and that the stiffening and bridging binding modes can co-exist in certain ionic conditions. Thus, our results clearly identify two distinct but switchable mechanisms of H-NS binding to DNA, which has not been reported previously. During pathogenesis, magnesium environments change considerably [22, 23]. Therefore, we proposed that the subsequent change in H-NS binding mode could assist transcription factors to relieve silencing of horizontally acquired genes and promote expression of virulence factors.

5.2. Methods

Magnetic-tweezer Manipulation of H-NS-DNA complex

The magnetic-tweezer setup and DNA attaching process are the same as described in previous chapters. After the persistence length A was tested to be in the right range (50 ± 3nm), H-NS was added under the channel in different buffer conditions and during the time, a force, which is large enough to prevent DNA folding or stiffening effect, was applied. The “stiffening buffer” contained 10mM Tris and different concentration of potassium chloride in a pH = 7.4 condition (no magnesium ion). The “folding buffer” contained 10mM Tris, 50mM potassium chloride and different concentration of magnesium chloride in a pH = 7.4 condition. To study the ionic influence on H-NS functions, we varied the potassium ion concentration in the “stiffening buffer” and the magnesium concentration in the “folding buffer". Furthermore, we also replace the magnesium ion with calcium ion to see whether it is solely the charge that matters.

Atomic Force Microscope imaging

The complexes of H-NS-DNA were formed by incubating 20 ng linear Phix174 DNA with H-NS in different kinds of “stiffening” and “folding” buffers for 20 minutes at room temperature (~24ºC). The mixture was then deposited onto the glutaraldehyde-treated mica for another 20 minutes. Then, the mica was gently rinsed with deionized water, and dried by a steady stream of nitrogen. Images were acquired by using Agilent PicoPlus.

5.3. Results

Ionic strength and magnesium ion alter the mode of H-NS binding to DNA.

We noticed that the reaction buffer used by Dame et al. contained 10 mM $MgCl_2$ [17, 18], whereas the one used by Amit et al. did not contain divalent cations [19]. We thus hypothesized that the discrepancy between the stiffening mode [19] and bridging mode [17, 18] of H-NS binding to DNA might result from the differences in buffer conditions rather than in the experimental design. Our results indicate that this hypothesis is valid.

We first measured force-extension curves in buffers similar to those used by Amit et al.: 10 mM Tris buffer (pH = 7.4) with various concentrations of KCl (5, 50, 100, and 200 mM). The H-NS concentration was fixed at 600 nM. Under these conditions, we obtained similar results to those reported in [19], as shown in Fig. 5.1 DNA stiffening, as evidenced by increased extension under the respective forces, was observed in 5, 50 and 100 mM KCl buffer condition. Furthermore, the lower KCl concentration in buffer the stronger the stiffening effect can be observed (see red triangles in Fig. 5.1 (a)), and the stiffening effect was negligible in 200 mM KCl buffer where the force extension curves were identical in the absence and presence of H-NS (compare black squares and orange circles). At 200 mM KCl, H-NS is not

bound to DNA, as suggested by the overlapping F-E curve with naked DNA (Fig. 5.1 (a)). Furthermore, the AFM imaging shows a grainy surface, suggesting that there may be many free proteins in the solution (Fig. 5.3 e-f). Lastly, no DNA folding (bridging) was apparent under forces ranging from 0.05 pN up to 20 pN under all conditions examined.

We next investigated the binding of H-NS to DNA in buffers similar to those used by Dame et al., i.e., 10 mM Tris buffer (pH 7.4) containing 50 mM KCl, 10 mM $MgCl_2$ (17). The H-NS concentration was again fixed at 600 nM. Interestingly, dramatic DNA folding occurred in this magnesium-containing buffer under small forces, but no folding is observed in the absence of $MgCl_2$. Fig. 5.1 (b) shows the real time course of DNA extension under different forces. We first decreased forces step by step and we recorded DNA extension for one or a few minutes at each step. There was no dramatic folding at forces larger than 0.2 pN. At 0.2 pN force, the extension of DNA was substantially reduced, indicating that a large-scale folding occurred (shown in dark blue). Unfolding occurred at 0.43 pN (yellow curve), at which most of the folded DNA was unfolded gradually. At a force of 0.73 pN, the DNA was completely unfolded (for completely unfolded, we mean that the two magenta curves before folding and after unfolding have the same height). When these data were plotted into a force-extension curve (Fig. 5.1 (c)), the DNA extension curve overlapped that of naked DNA before folding at 0.2 pN (indicated as a red dashed arrow). This result suggests that before folding (or bridging), DNA has similar rigidity as the naked DNA, but after folding, it becomes less extended. These observations are in agreement with

the DNA bridging experiments as reported earlier [17, 18]. In addition, the unfolding force was found to be dependent on the incubation time of H-NS-DNA in a folded state, the longer the duration, the larger the unfolding force (up to a few pN).

Magnesium acts as a switch between stiffening and bridging.

In the previous experiment shown in Fig. 5.1, we demonstrated that H-NS binding to DNA led to stiffening in the absence of $MgCl_2$ and bridging in the presence of 10 mM $MgCl_2$. This suggests an important role of magnesium in mediating the switching from one binding mode to the other, which has not been reported previously. As a result, we examined the switching between the two binding modes in detail by gradually changing the concentration of magnesium in buffers containing 10 mM Tris (pH 7.4), 50 mM KCl, 600 nM H-NS. Fig. 5.1 (d) shows the force-extension curves prepared by increasing $MgCl_2$ concentration from 0-10 mM using the same DNA during the scanning process. At each concentration, the DNA extension was recorded under different forces. Our results indicate that as the magnesium concentration increased, DNA rigidity decreased (i.e. the DNA was less extended at each respective force). At 5 mM magnesium (orange triangles), folding occurred in the presence of ~0.1 pN force. This bridged DNA was then completely unfolded at a larger force of ~7 pN, under which the $MgCl_2$ concentration was increased to 10 mM. The force was then gradually decreased in the 10 mM $MgCl_2$ buffer (purple stars) and dramatic bridging occurred at a larger stretching force (> 0.2 pN; purple dashed arrow). In

summary, stiffening of DNA was observed at 0-5 mM magnesium, whereas folding (bridging) was observed in 5-10 mM. At 5 mM, both stiffening (force > 0.1 pN) and bridging were observed (force ≤ 0.1 pN).

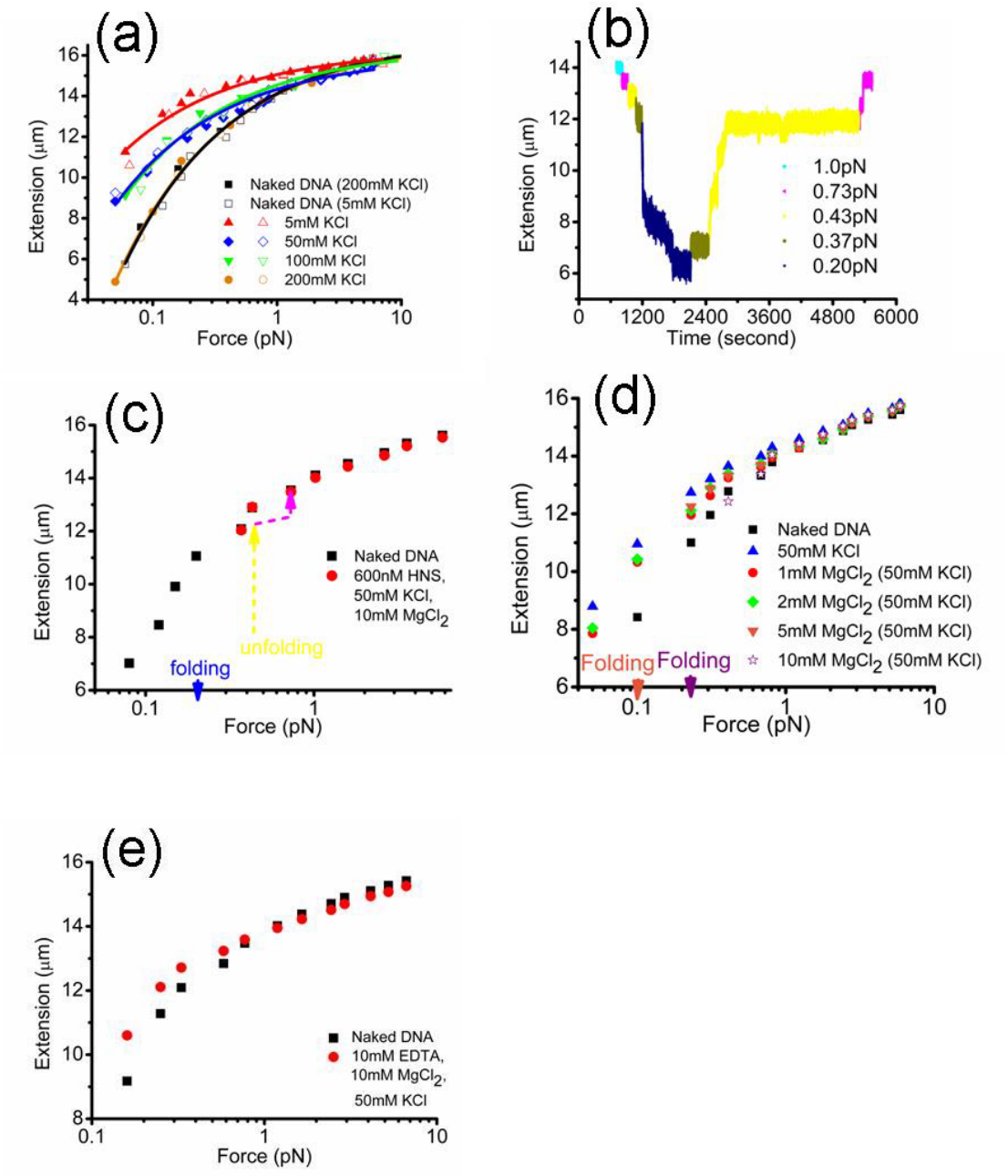

Fig. 5.1 Magnesium dependent binding modes of H-NS.

(a) Force-extension curve of DNA in the absence of magnesium where DNA stiffening occurs. Two independent data sets are shown (open and closed symbols) at each KCl concentration.

The solid and open squares are the reference curves of DNA in buffer alone containing 5 mM KCl and 200 mM KCl, respectively. The DNA becomes less stiff (less extended at respective forces) as the KCl concentration increases. The H-NS concentration is fixed at 600 nM.

(b) Time course of DNA folding/unfolding in the presence of 50 mM KCl, 10 mM $MgCl_2$, 600 nM H-NS. Folding occurs at 0.2 pN (dark blue line) and unfolding occurs at 0.43 pN (yellow line). Complete unfolding occurred at 0.73 pN. The two magenta colors before folding and after unfolding are at the same extension.

(c) Force-extension curve corresponding to (b). Before folding, the DNA has similar rigidity to naked DNA. The blue arrow indicates the folding at 0.2 pN (shown in panel (b) as dark blue). The yellow and magenta arrows indicate 0.43 pN and 0.73 pN, respectively, where unfolding was observed. Panel (b) is a representative example of many experiments that were performed. In five similar experiments, folding occurred under ~0.2 pN of force and subsequent unfolding occurred under ~0.4 pN. In three additional experiments, folding occurred under ~1 pN and subsequent unfolding occurred under a few pN of force (data not shown).

(d) Switching H-NS from stiffening to bridging mode by increasing the concentration of $MgCl_2$. Apparent stiffening occurred at $\leq$5 mM $MgCl_2$, i.e., extension is greater than that of the naked DNA at the same force. Folding (bridging) occurred at $\geq$5 mM $MgCl_2$. The orange arrow indicates folding at ~0.1 pN in the presence of 5 mM $MgCl_2$. This bridged DNA was then completely unfolded at a larger force of ~7 pN, during which $MgCl_2$ concentration was increased to 10 mM. The force was then incrementally reduced in the 10 mM $MgCl_2$ buffer (purple stars) and bridging occurred at a higher stretching force (> 0.2 pN; purple arrow. Stiffening (> 0.1 pN) and folding ($\leq$ 0.1 pN) co-exist at 5 mM $MgCl_2$. The H-NS concentration is fixed at 600 nM.

(e) Effects of chelation of magnesium by EDTA. The extension of DNA 10 mM Tris (pH = 7.4), 50 mM KCl, 10 mM $MgCl_2$, and 600 nM H-NS (red solid circles) is longer than that in the absence of H-NS (black squares), indicating that the DNA becomes stiffer.

Stiffening results from cooperative H-NS polymerization along DNA.

We observed DNA stiffening in KCl and $MgCl_2$ buffers of less than 100 mM and 5 mM, respectively (Fig. 5.1 (a) and (d)). Yet, the mechanism of DNA binding by H-NS that results in stiffening remained unclear. We considered the following two possibilities: 1) random binding with high occupation number (i.e., the linear density of bound protein is large) could lead to stiffening if each binding event can locally stiffen the DNA backbone [24], or 2) cooperative polymerization along the DNA leading to a more rigid H-NS-DNA co-filament. To investigate these possibilities, we performed AFM imaging of the DNA-H-NS complexes in the DNA stiffening buffers employed previously. Fig. 5.3 (a) – (d) shows four representative AFM images of 0.14 nM DNA incubated with 600 nM H-NS for 30 minutes (Fig. 5.3 (a) and (b)) and for 240 minutes (Fig. 5.3 (c) and (d)) in 5 mM KCl, 0 mM $MgCl_2$. Under this condition, the ratio of H-NS monomer per base pair is 0.8. Panels (a) and (b) reveal that H-NS polymerized along the DNA and formed disconnected islands (the brighter part along DNA), suggesting that a nucleation event was required for the extension of the protein coated regions. Panels (c) and (d) indicate that at longer incubation times, the disconnected regions merge (the previous brighter parts of DNA seems to extend), leading to fully coated DNA. In panels (c) and (d) completely uncoated DNA is also

visible. This result is in complete agreement with a nucleation polymerization mode, where H-NS protein tends to condense at nucleation sites and polymerize along DNA. Thus, our results support the second possibility, that under DNA stiffening conditions, H-NS cooperatively polymerizes along DNA.

Fig. 5.3 panels (e) – (h) show four representative AFM images of DNA incubated with 600 nM H-NS for 40 minutes in 50 mM KCl and 0 mM $MgCl_2$ (Fig. 5.3 (e) and (f)) and 1 mM $MgCl_2$ (Fig. 5.3 (g) and (h)). Under these conditions, magnetic tweezer experiments showed that the DNA was stiffened, and no folding (bridging) event was observed (Fig. 5.1 (a) blue diamond and (d) red circle). In accordance, with the observations, the majority of DNA in the imaging experiment was found in extended form. The rigid islands were still seen, but with lower contrast than is observed inFig. 5.3 (a) – (d). On rare occasions, some DNA bundling formation was observed (see red arrows in panels Fig. 5.3 (f) and (h)). These bundle formations were not observed in the magnetic tweezer experiments, most likely because they are rare events. Furthermore, comparing with panels Fig. 5.3 (a) – (d), the mica surface became rougher and the DNA image had poor contrast. This was likely due to reduced H-NS binding to DNA; therefore more H-NS proteins in solution are available to bind to the mica surface, leading to surface roughness. We also attempted to image DNA in 200 mM KCl, 0 mM $MgCl_2$. Under these conditions, the mica surface was fully coated with H-NS protein, leading to very poor imaging contrast of DNA (data not shown).

Taken together, these observations indicate that as the KCl concentration increases, protein occupation on DNA decreases, and H-NS interaction with the mica

surface is favored. Furthermore, it suggests an electrostatic nature of H-NS binding to DNA in the range of 0-1 mM magnesium, where the DNA stiffening mode of binding predominates.

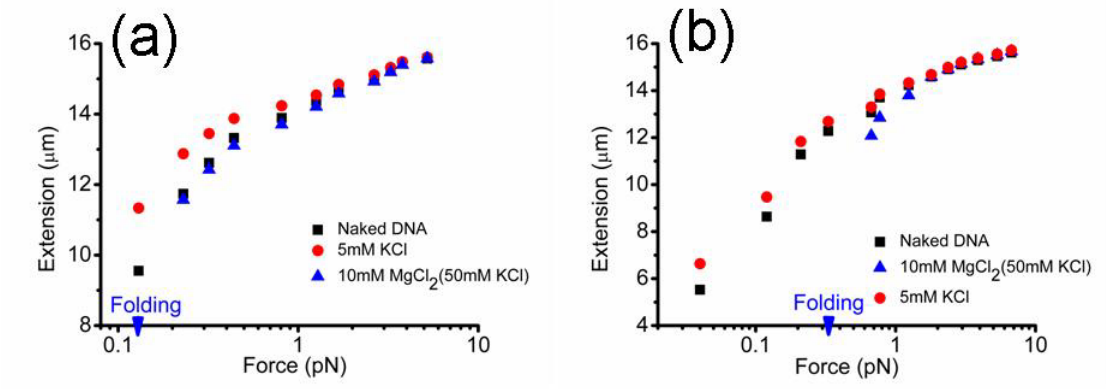

Fig. 5.2 H-NS interconverts between bridging and stiffening modes without being released from DNA.

(a) Switching from stiffened DNA in 600 nM H-NS, 5 mM KCl, 0 mM $MgCl_2$ to bridging buffer in the absence of H-NS (0 mM H-NS, 50 mM KCl, 10 mM $MgCl_2$) resulted in bridging. The blue arrow on the force-axis indicates theforce where the folding occurred.

(b) Switch from bridged DNA in (600 nM H-NS, 50 mM KCl, 10 mM $MgCl_2$) to stiffening buffer in the absence of H-NS (0 mM H-NS, 5 mM KCl, 0 mM $MgCl_2$) resulted in stiffening. Thus, it is apparent that H-NS is capable of interconverting between the stiffening and bridging forms without dissociation from DNA.

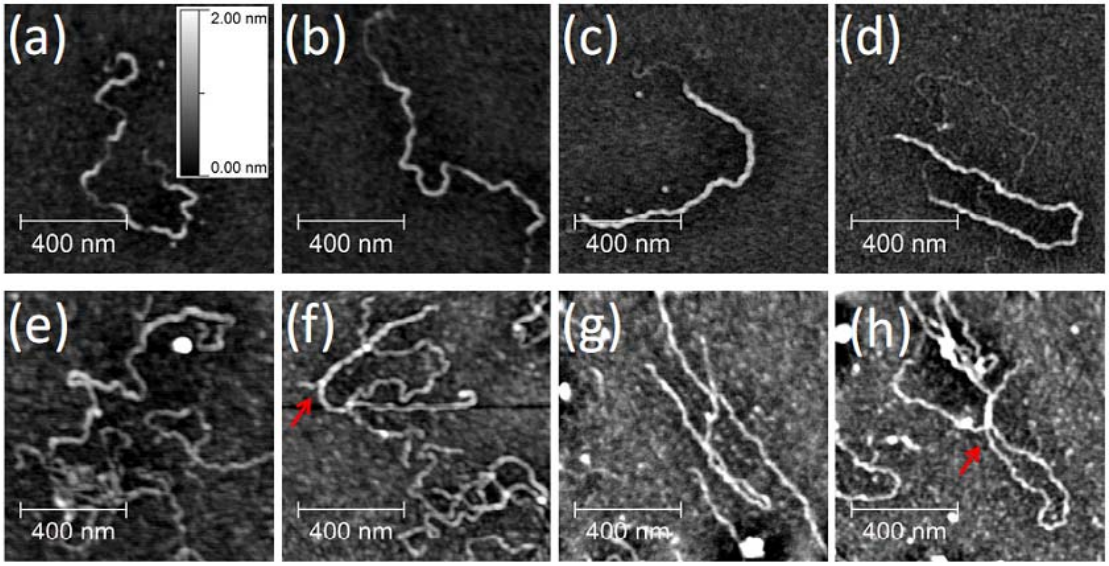

Fig. 5.3 Imaging of DNA–H-NS complexes in the absence of or with low $MgCl^2$ concentration using Atomic Force Microscopy.

(a-b) 5 mM KCl, 0 mM $MgCl_2$, incubated for 40 minutes.

(c-d) 5 mM KCl, 0 mM $MgCl_2$, incubated for 4 hours. The brighter regions indicate the H-NS bound region, while the darker regions indicate the naked DNA backbone.

(e-f) 50 mM KCl, 0 mM $MgCl_2$, and (G-H) 50 mM KCl, 1 mM $MgCl_2$, incubated for 40 minutes. The majority of DNA molecules are in an extended form in panels.

During folding (bridging), large DNA hairpin structures form.

It was therefore of interest to determine what contributed to the DNA folding signals observed in the folding buffers containing $MgCl_2$. In Fig. 5.4 panels (a) – (d) (image obtained from 50mM KCl and 5mM $MgCl_2$), small end-loops can be observed in the linear hairpins structures of DNA. The linear hairpin structures clearly indicate the formation of large-scale DNA bridging, and the end-loops are likely resulted from the competition between the bridging energy and the bending energy of DNA. In

addition to linear DNA hairpins, circular DNA conformations were also found, even though linear DNA was used in the reaction.

When the $MgCl_2$ was increased to 10 mM, the hairpins and circular conformations were similar to those obtained with 5 mM $MgCl_2$ (Fig. 5.4 (e) – (g)), but the images were much sharper because the mica surface was cleaner. In some of the circular forms, "holes" were evident (e.g., Fig. 5.4 (e)), indicating that these circular forms were still bridged DNA molecules. Bridging can form two different structures as the orientation at two remote DNA sites varies as they meet prior to bridging. If their orientations were anti-parallel (or nearly so), bridging favored the formation of hairpins (left, Fig. 5.4 (h)). On the other hand, if they were parallel (or nearly so), bridging favored formation of the circular conformations (right, Fig. 5.4 (h)).

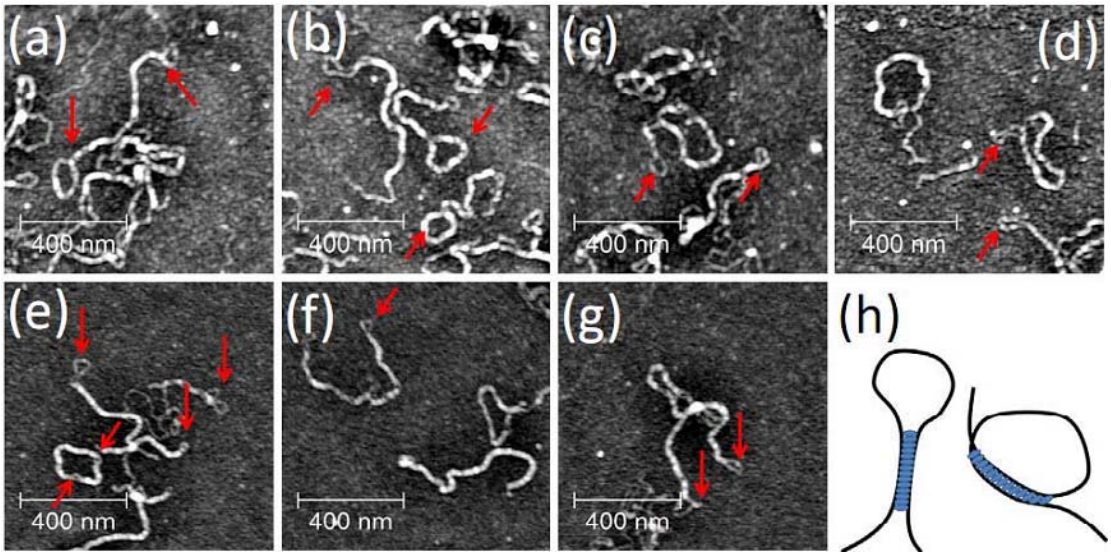

Fig. 5.4 Imaging of DNA–H-NS complexes in the bridging binding mode.
(a-d) 50 mM KCl and 5 mM $MgCl_2$.

(e-g) 50 mM KCl and 10 mM $MgCl_2$. Incubation time was fixed at 40 minutes, and the H-NS concentration was 600 nM. Large linear hairpin forms and circular forms were observed.
(h) Two boundary conformations of the seeding loop: almost anti-parallel (left), and almost parallel (right).

5.4. Discussion

We have shown that H-NS possesses two distinct DNA binding modes, one stiffens DNA and the other bridges DNA, and magnesium acts as a switch between the two modes. Our results have two important implications 1) the previous discrepancy between DNA bridging and DNA stiffening was due to the absence or presence of magnesium, respectively and 2) these two binding modes of H-NS could play distinct roles in genome organization (DNA compaction) and gene silencing. Genome packaging by H-NS is likely relevant to non-specific DNA bridging, since it can effectively reduce the dimensions of DNA molecules. At this moment, the role of DNA stiffening by H-NS binding under low $MgCl_2$ concentrations remains unclear. As shown in Fig. 5.3 (a) – (d), the decoration of DNA by H-NS initiates at discrete sites at early times, suggesting a sequence specificity to the early binding (e.g., it is known that H-NS preferentially binds to A-T rich DNA). At low $MgCl_2$ concentrations, polymerizing of H-NS may start from these nucleation sites, and the H-NS coating region may be extended to cover a larger distance including promoter regions. Therefore, one obvious possibility is that by coating along DNA in the DNA

stiffening mode of binding, promoter regions become less accessible to RNA polymerase leading to gene silencing.

The stiffening mechanism was revealed by the AFM images: H-NS polymerizes along DNA starting from a few nucleation sites, and finally merges together leading to fully coated DNA. There are two possible steps for this cooperative process: 1) H-NS-coated regions grow in islands before merging (Fig. 5.3 (a) and (b)), and 2) after a few hours of incubation, the DNA is either naked or fully coated (Fig. 5.3 (c) and (d)). The stiffening mode of binding is sensitive to the concentration of KCl. At high KCl (>100mM) concentrations, less binding is evident, thus more H-NS protein is in solution and can bind to the mica surface. This suggests a simple electrostatic nature of the stiffening binding mode.

The bridging mode is distinct from the stiffening mode. Bridging leads to formation of linear hairpin structures or circular conformations (Fig. 5.4). Bridging is also likely to be cooperative, as evidenced by the observation that DNA is either bridged or naked in 50 mM KCl and 10 mM $MgCl_2$ (naked DNA not shown). Interestingly, at a fixed concentration of 50 mM KCl, increasing the $MgCl_2$ concentration up to 10 mM enhances binding (compare Fig. 5.4 (a) – (d) and (e) – (g)). This implies a non-trivial role of magnesium in coordinating H-NS binding to DNA. $CaCl_2$ can also promote the switch to the bridging binding mode (not shown). At this moment, the mechanism behind the switching of H-NS binding from polymerizing to bridging in the presence of $MgCl_2$ or $CaCl_2$ remains unclear. H-NS exists as a dimer and has the ability to self-associate to form higher order oligomers. Therefore we

suspect that the Mg^{2+} or Ca^{2+} ions exert their effects by altering the oligomerization state of H-NS in solution. This possibility is currently being tested in our laboratory.

Our finding of the magnesium-mediated switching between DNA stiffening and DNA bridging may have important implications in the biological functions of H-NS. It is known that during pathogenesis, magnesium levels change considerably [22, 23]. Consequently, it is logical that a change in magnesium level *in vivo* may drive H-NS switching from one binding mode to the other. Therefore, it will be of interest to investigate whether relief of H-NS-silenced, horizontally acquired genes and hence promotion of expression of virulence factors is a function of the H-NS binding mode. Numerous regulatory proteins are involved in de-repressing the genes silenced by H-NS [25]. Therefore, relief of silencing is likely a function of both the binding mode and the respective antagonizing proteins. Hence, investigation of competition of transcription factors with H-NS for binding to DNA under various magnesium levels will be necessary. A logical candidate for such studies is SsrB, a protein that combines the roles of H-NS antagonist and transcriptional activator involved in expression of diverse genes located on Salmonella pathogenicity island 2 [15]. Thus, we suggest that the magnesium switch may have important effects on virulence gene expression.

5.5. Supplementary Data

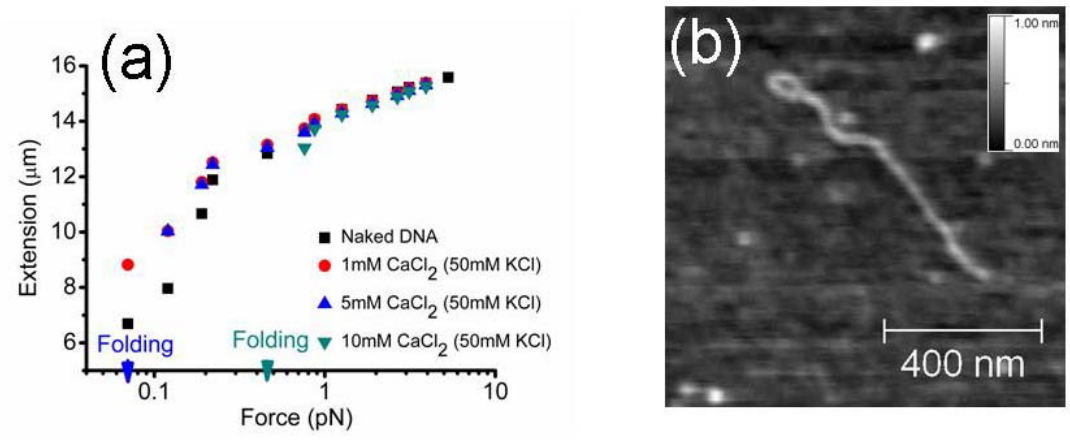

Fig. 5.5 Calcium substitutes for magnesium in stimulating the bridging/polymerization switch.

(a) DNA is folded when the protein solution contains 50 mM KCl and 10 mM $CaCl^2$ at < 0.2 pN force.

(b) A representative image is shown indicating that the folded DNA molecules are also organized into hairpin structures.

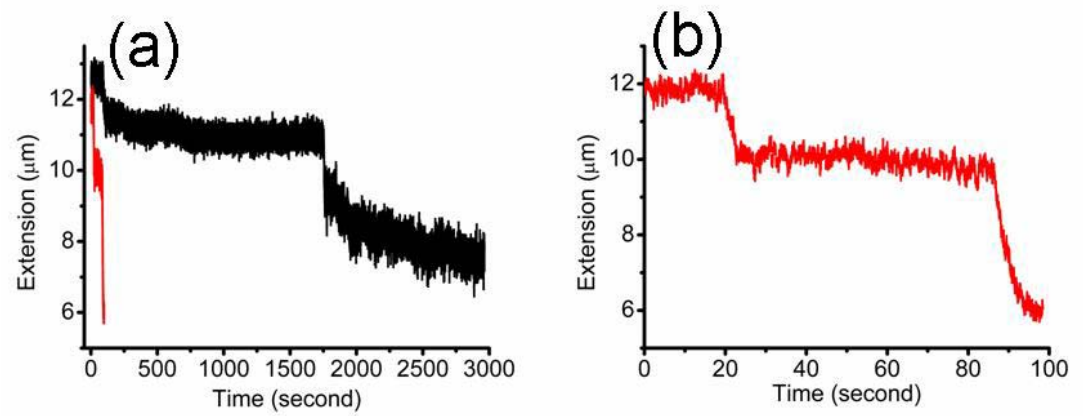

Fig. 5.6 Increasing the H-NS concentration dramatically reduces the DNA folding kinetics.

(a) The folding time course of DNA in the presence of 2.4 μM H-NS in 10 mM Tris (pH 7.4)

containing 50 mM KCl, 10 mM $MgCl^2$ is shown in black, the time course in the presence of 600 nM H-NS in the same buffer is shown in red.

(b) Magnification of the red time course (low [H-NS]). Compared to the folding observed in the presence of 600 nM H-NS, the folding speed in 2.4 μM H-NS is reduced by > 30-fold.

5.6. References

[1] M. S. Luijsterburg, M. C. Noom, G. J. L. Wuite, and R. T. Dame, J. Struct. Biol. **156**, 262 (2006).

[2] D. C. Grainger, D. Hurd, M. D. Goldberg, and S. J. W. Busby, Nucleic Acids Res. **34**, 4642 (2006).

[3] S. Lucchini, G. Rowley, M. D. Goldberg, D. Hurd, M. Harrison, and J. C. D. Hinton, PLoS Pathog. **2**, e81 (2006).

[4] W. W. Navarre, S. Porwollik, Y. Wang, M. McClelland, H. Rosen, S. J. Libby, and F. C. Fang, Science **313**, 236 (2006).

[5] T. Oshima, S. Ishikawa, K. Kurokawa, H. Aiba, and N. Ogasawara, DNA Res. **13**, 141 (2006).

[6] J. T. Wade, K. Struhl, S. J. W. Busby, and D. C. Grainger, Mol. Microbiol. **65**, 21 (2007).

[7] V. Bloch, Y. S. Yang, E. Margeat, A. Chavanieu, M. T. Auge, B. Robert, S. Arold, S. Rimsky, and M. Kochoyan, Nat. Struct. Biol. **10**, 212 (2003).

[8] C. P. Smyth, T. Lundback, D. Renzoni, G. Siligardi, R. Beavil, M. Layton, J. M. Sidebotham, J. C. Hinton, P. C. Driscoll, C. F. Higgins, and J. E. Ladbury, Mol.

Microbiol. **36**, 962 (2000).

[9] D. Esposito, A. Petrovic, R. Harris, S. Ono, J. F. Eccleston, A. Mbabaali, I. Haq, C. F. Higgins, J. C. Hinton, P. C. Driscoll, and J. E. Ladbury, J. Mol. Biol. **324**, 841 (2002).

[10] A. Spassky, S. Rimsky, H. Garreau, and H. Buc, Nucleic Acids Res. **12**, 5321 (1984).

[11] R. Spurio, Durrenberger, M., Falconi, M., La Teana, A., Pon, C.L., and Gualerzi, C.O., Mol. Gen. Genet. **231**, 201 (1992).

[12] J. Stavans, and A. B. Oppenheim, Phys. Biol. **3**, R1 (2006).

[13] C. J. Dorman, Nat. Rev. Microbiol. **5**, 157 (2007).

[14] A. K. Heroven, G. Nagel, H. J. Tran, S. Parr, and P. Dersch, Mol. Microbiol. **53**, 871 (2004).

[15] W. W. Navarre, M. McClelland, S. J. Libby, and F. C. Fang, Genes Dev. **21**, 1456 (2007).

[16] D. Walthers, R. K. Carroll, W. W. Navarre, S. J. Libby, F. C. Fang, and L. J. Kenney, Mol. Microbiol. **65**, 477 (2007).

[17] J. C. Perez, T. Latifi, and E. A. Groisman, J. Biol. Chem. **283**, 10773 (2008).

[18] R. T. Dame, C. Wyman, and N. Goosen, Nucleic Acids Res. **28**, 3504 (2000).

[19] R. T. Dame, M. C. Noom, and G. J. L. Wuite, Nature **444**, 387 (2006).

[20] R. Amit, A. B. Oppenheimy, and J. Stavans, Biophys. J. **84**, 2467 (2003).

[21] R. T. Dame, and G. J. L.Wuite, Biophys. J. **85**, 4146 (2003).

[22] R. Amit, A. B. Oppenheimy, and J. Stavans, Biophys. J. **87**, 1392 (2004).

[23] N. Martin-Orozco, N. Touret, M. L. Zaharik, E. Park, R. Kopelman, S. Miller, B. B. Finlay, P. Gros, and S. Grinstein, Mol. Biol. Cell **17**, 498 (2006).

[24] K. M. Papp-Wallace, and M. E. Maguire, J. Bacteriol. **190**, 6509 (2008).

[25] J. Yan, and J. F. Marko, Phys. Rev. E Stat. Nonlin. Soft Matter Phys. **68**, 011905 (2003).

Chapter 6. Conclusion

DNA architectural protein has long been of interest in biophysical research. Many newly invented techniques, such as AFM, magnetic tweezers, optical tweezers, have been applied in studying the interactional processes and functional mechanisms between DNA and proteins. According to their effects on DNA, the architectural proteins can be generally classified into 3 groups, that is: DNA wrapper, DNA bender and DNA bridger. TEM and AFM have given clear and convincing topographic images for each kind, and the magnetic tweezers as well as optical tweezers provide useful information related to the interacting process, especially the critical force of DNA wrapper, changes of DNA persistence length induced by DNA bender, and the unfolding force of DNA bridger. Moreover, the interaction process varies for different proteins. It may happen in a gradual manner in which the DNA length is reduced at a slow speed, while another condition is also possible where a sudden decrease of DNA length occurs in less than 0.1 second. Other noteworthy information includes the folding step, switchable function and meta-stable status.

In this research, we explored 3 kinds of proteins coming from two domains: virus and bacteria; and revealed some basic roles these NAP played in genomic compaction and regulation.

The VP15 from white spot syndrome virus shows the simplest function among the 3 proteins where it is able to highly condense DNA. This is predictable since

VP15 has a large pI value of 13.2 and this indicates that it can greatly neutralize the negative charges of DNA by canceling the static repulsive force. In the magnetic tweezer experiment, at concentration of 66 nM, VP15 could significantly compact DNA against force as large as 5 pN and the critical force decreases as the concentration of VP15 is reduced (Fig. 4.2 in Chapter IV).

Sometimes, a meta-stable folding status appeared in which folding-and then-self-unfolding behavior presents under a constant force (Fig. 4.2 C in Chapter IV). The flower-shaped DNA-protein structures from AFM images further confirm the strong ability of VP15 in condensing DNA and in connecting remote sites leading to loop formation, and these may explain the fast and sudden reduction in DNA length showed in the magnetic tweezers experiment (Fig. 4.4 in Chapter IV).

The single chain IHF (scIHF) and its mutants (scIHF-K45αE) which serve as DNA benders are able to bend DNA to certain angle under the mediation of Mg^{2+}. Therefore, their regulating mechanism seems more complicated than VP15. The wild-type IHF, single-chain IHF and single-chain IHF mutant can respectively introduce different bending angles distribution on DNA in the absence of Mg^{2+} (Fig. 3.7 in Chapter III). However, when Mg^{2+} is present, the single-chain IHF exhibits a bending ability similar to the single-chain IHF as the Mg^{2+} concentration increases (Fig. 3.8 in Chapter III). This implies the potential application of the single-chain IHF mutant as a Mg^{2+} mediated switch in bio-engineering.

The most notable architectural protein in our research is H-NS, which can induce two distinctly different DNA behaviors (DNA stiffening and DNA folding) based on

the ionic condition of the buffer (Fig. 5.1 in Chapter V). These two binding modes were previously considered mutually exclusive, and they were the source of an unresolved controversy. In our study, Mg^{2+}, when its concentration is larger than 5 mM, can switch the function of H-NS from DNA stiffening to DNA folding (Fig. 5.2 in Chapter V).

The stiffening binding mode has been ignored in the field, possibly because it was seldom reported. Numerous studies on the bridging mode resulted in it becoming the canonical form when investigators discuss binding mechanism of H-NS to DNA. However, it has been known that the physiological concentration of magnesium in cells is approximately 1 μM, calcium is approximately 100 – 300 nM, and in addition of multivalent polyamines. The ionic concentration was lower than the switching concentration that we found in our experiments (5 mM Mg^{2+}). The fact indicates that it is the stiffening mode, instead of the folding mode, that plays an important role in genomic regulation in cell growth.

The hypothesis was partially supported by our recent experiments of H-NS reaction to pH and temperature condition. The stiffening binding mode of H-NS was sensitive to changes in temperature ranging from 24 ºC to 37ºC, i.e., elevation of the temperature decreased the stiffening effects; at 37 ºC, no stiffening was apparent. In contrast, for the bridging binding mode, H-NS was not sensitive to temperature changes. Large scale bridging at ~0.3 pN was still evident at 37ºC. As for the pH dependence, increasing the pH from 6.5 to 8 decreases the stiffening effect but the not the bridging mode. Therefore, we suggest that the previously ignored stiffening mode

is most likely to be physiologically relevant, since it is the sensitive mode that responds to environmental stimuli that alter H-NS behavior. Our research presents a paradigm shift in the way of thinking about how H-NS works. But we also understand the limitation in our experiments, since the *in vitro* buffer condition is largely different from the complicated *in vivo* condition where molecular crowding (as mentioned in the Chapter I) and other charged molecules are present. We cannot exclude the possibility that bridging binding mode is also physiologically relevant, and future research should lay more importance in mimicking the *in vivo* condition.

Many questions were raised by this research: such as whether both binding modes are physiological relevant, whether one mode is preferred, whether the switching function is a potential mechanism for cell to react to the environmental change, and how the H-NS interaction differs when Mg^{2+} is present.

All the three researches focused on the DNA interaction with only one protein at a time. However, in an organism, there are hundreds to thousands of proteins inside a cell, and it would not be a surprise for them to cooperate in modulating genomic structure and perform regulatory functions. It may be two or even more proteins that are required to ensure transcription is performed exactly, and the integrity of genomic information is well preserved.

Our latest result indicates that SsrB protein, another DNA binding protein, can repress the H-NS stiffening effect, leading to condensation of DNA in the absence of Mg^{2+}. Biological experiments from our cooperator suggest that SsrB can drive H-NS away from DNA and then attach to binding sites. Our preliminary experiment showed

a much larger unfolding force of DNA loop introduced by SsrB compared to those introduced by H-NS. Therefore, the SsrB combines the roles of H-NS antagonist and transcriptional activator in regulating the expression of diverse genes. Related works are now being carried out in our group.

List of publications

Liu, Y.J., H.Chen, L.J. Kenney, and J. Yan (2010). "A divalent switch drives H-NS/DNA-binding conformations between stiffening and bridging modes." Genes & Development 24:339-344.

Yingjie Liu; Jinlu Wu, Ph.D, Hu Chen, Ph.D; Choy L Hew, Ph.D; Jie Yan, Ph.D. “DNA condensates organized by the capsid protein VP15 in White Spot Syndrome Virus”, Virology. (In Processing)

Bao, Q., H. Chen, **Y.J. Liu**, J. Yan, P. Dröge, and C.A. Davey (2007). "A Divalent Metal-mediated Switch Controlling Protein-induced DNA Bending." Journal of Molecular Biology **367**(3): 731-740.